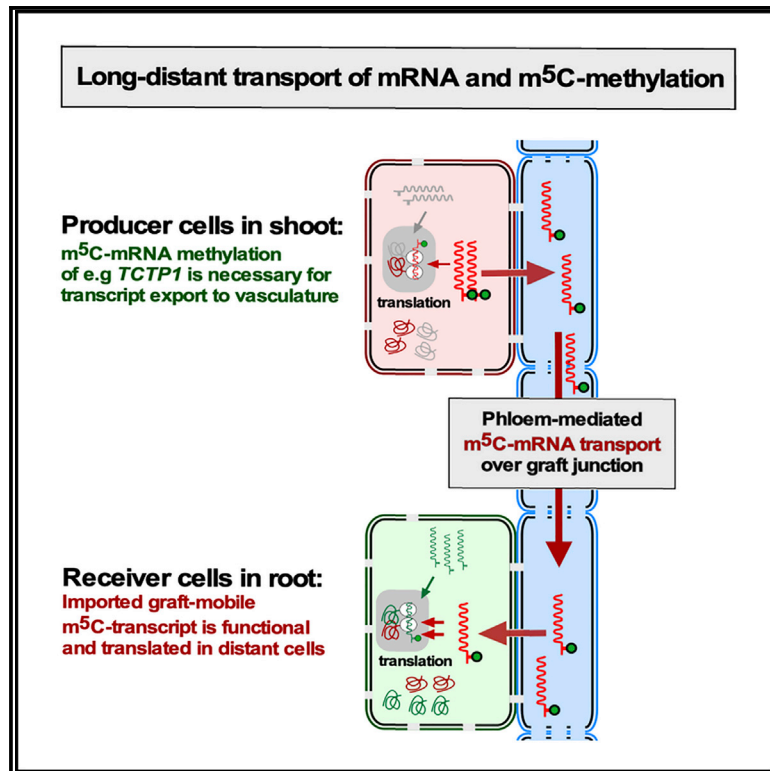


# Current Biology

## $m^5C$ Methylation Guides Systemic Transport of Messenger RNA over Graft Junctions in Plants

### Graphical Abstract



### Authors

Lei Yang, Valentina Perrera, Eleftheria Saplaoura, ..., Auguste Genovesio, Vincent Colot, Friedrich Kragler

### Correspondence

kragler@mpimp-golm.mpg.de

### In Brief

In plants, thousands of messenger RNAs move to distant body parts to potentially act as systemic signals. Yang, Pererra, et al. show that 5-methylcytosine ( $m^5C$ ) modification of mobile RNA plays a crucial role in facilitating their transport and present evidence that mobile  $m^5C$ -modified *TCTP1* is translated in target cells and changes root growth.

### Highlights

- $m^5C$  methylation is highly enriched in transcripts moving from shoot to root
- *TCTP1* and *HSC70.1* mRNAs are not graft mobile in RNA methylation-deficient mutants
- *TCTP1* is translated after transport in distinct root cells and affects root growth



# m<sup>5</sup>C Methylation Guides Systemic Transport of Messenger RNA over Graft Junctions in Plants

Lei Yang,<sup>1,8</sup> Valentina Perrera,<sup>2,8,9</sup> Eleftheria Saplaoura,<sup>1</sup> Federico Apelt,<sup>1</sup> Mathieu Bahin,<sup>2</sup> Amira Kramdi,<sup>2</sup> Justyna Olas,<sup>3</sup> Bernd Mueller-Roeber,<sup>3</sup> Ewelina Sokolowska,<sup>1</sup> Wenna Zhang,<sup>1,4</sup> Runsheng Li,<sup>5</sup> Nicolas Pitzalis,<sup>6</sup> Manfred Heinlein,<sup>6</sup> Shoudong Zhang,<sup>5,7</sup> Auguste Genovesio,<sup>2</sup> Vincent Colot,<sup>2</sup> and Friedrich Kragler<sup>1,10,\*</sup>

<sup>1</sup>Max-Planck-Institute of Molecular Plant Physiology, Wissenschaftspark Golm, Am Mühlenberg 1, 14476 Golm, Germany

<sup>2</sup>Institut de Biologie de l'Ecole Normale Supérieure (IBENS), CNRS UMR8197, INSERM U1024, PSL Research University, 75230 Paris, France

<sup>3</sup>Institute of Biochemistry and Biology, University of Potsdam, Department of Molecular Biology, Karl-Liebknecht-Strasse 24-25, Haus 20, 14476 Potsdam, Germany

<sup>4</sup>China Agricultural University, 17 Qinghua East Road, 100080 Haidian, Beijing, China

<sup>5</sup>Department of Biology, Hong Kong Baptist University, Hong Kong, Hong Kong SAR, China

<sup>6</sup>Institut de Biologie Moléculaire des Plantes du CNRS, IBMP-CNRS UPR2357, 12, rue du Général Zimmer, 67084 Strasbourg, France

<sup>7</sup>Centre for Soybean Research, Partner State Key Laboratory of Agrobiotechnology and School of Life Sciences, The Chinese University of Hong Kong, Shatin, Hong Kong, Special Administrative Region, China

<sup>8</sup>These authors contributed equally

<sup>9</sup>Present address: Department of Molecular Medicine, Medical School, University of Padua, via Gabelli 63, 35121 Padua, Italy

<sup>10</sup>Lead Contact

\*Correspondence: [kragler@mpimp-golm.mpg.de](mailto:kragler@mpimp-golm.mpg.de)

<https://doi.org/10.1016/j.cub.2019.06.042>

## SUMMARY

In plants, transcripts move to distant body parts to potentially act as systemic signals regulating development and growth. Thousands of messenger RNAs (mRNAs) are transported across graft junctions via the phloem to distinct plant parts. Little is known regarding features, structural motifs, and potential base modifications of transported transcripts and how these may affect their mobility. We identified *Arabidopsis thaliana* mRNAs harboring the modified base 5-methylcytosine (m<sup>5</sup>C) and found that these are significantly enriched in mRNAs previously described as mobile, moving over graft junctions to distinct plant parts. We confirm this finding with graft-mobile methylated mRNAs *TRANSLATIONALLY CONTROLLED TUMOR PROTEIN 1 (TCTP1)* and *HEAT SHOCK COGNATE PROTEIN 70.1 (HSC70.1)*, whose mRNA transport is diminished in mutants deficient in m<sup>5</sup>C mRNA methylation. Together, our results point toward an essential role of cytosine methylation in systemic mRNA mobility in plants and that *TCTP1* mRNA mobility is required for its signaling function.

## INTRODUCTION

In plants, intercellular communication involves a high number of phloem-delivered proteins and RNAs, such as distinct microRNAs (miRNA), short interfering RNAs (siRNAs), and messenger RNAs (mRNAs). In different plant species, such as *Arabidopsis thaliana* (*Arabidopsis*), *Vitis vinifera* (grapevine), and *Cucurbitaceae* (cucumber, watermelon), thousands of protein-encoding mRNAs move over graft junctions to distant plant regions [1–4]. In watermelon/cucumber, *Nicotiana benthamiana*/tomato,

and *Arabidopsis* ecotype heterografts, hundreds of mRNAs are constitutively transferred to specific plant parts or in response to specific stress conditions [1–3]. Similarly, mRNAs targeting to specific subcellular compartments for localized translation are also detected in plants, fungi, and animals. Intracellular mRNA distribution is guided by mRNA zip codes interacting with mRNA-binding proteins [5–8]. This localized protein production can regulate cell polarity, patterning, and fate. However, for the vast majority of plant mRNAs delivered to distant tissues, we have no information regarding a potential signaling function, transport motif(s), or endogenous factors triggering their transport [9–11].

Long-distance transcript transport in plants might be explained by a non-specific promiscuous delivery system depending on abundance, size, or half-life, as suggested by bioinformatic analysis on graft-mobile *Arabidopsis* mRNAs [10]. However, protein-encoding transcripts are too large to diffuse via intercellular bridges built by plasmodesmata [12–15]. Independently of their size, highly expressed heterologous transcripts such as *GFP*, *YFP*, *GLUCURONIDASE (GUS)*, and *BASTA (bar)* [1, 16, 17] and truncated versions of endogenous mobile transcripts such as *Solanum tuberosum BELL-LIKE 5 (StBEL5)*, *Arabidopsis thaliana FLOWERING LOCUS T (FT)*, and *CHOLINE KINASE 1 (CK1)* [16, 18, 19] are unable to move to distant tissues over graft junctions. This indicates that specific motif(s) trigger mobility of endogenous transcripts. Mobile transcripts, such as *Arabidopsis thaliana GIBBERELLIC ACID INSENSITIVE (GAI)* [20] and *StBEL5*, seem to use polypyrimidine track protein binding sequences (PTB motif) to gain access to distant tissues [18, 20, 21]. However, this highly abundant and thus relatively unspecific PTB motif, composed of UUCUCUCUCUU bases [22], was not found to be significantly enriched in the *Arabidopsis* graft-mobile transcript populations [2, 10]. Another motif named tRNA-like sequence (TLS) seems to be significantly enriched, as it is predicted in approximately 12% and 7.5% of mobile transcripts of *Arabidopsis thaliana* and *Vitis vinifera*, respectively [2].



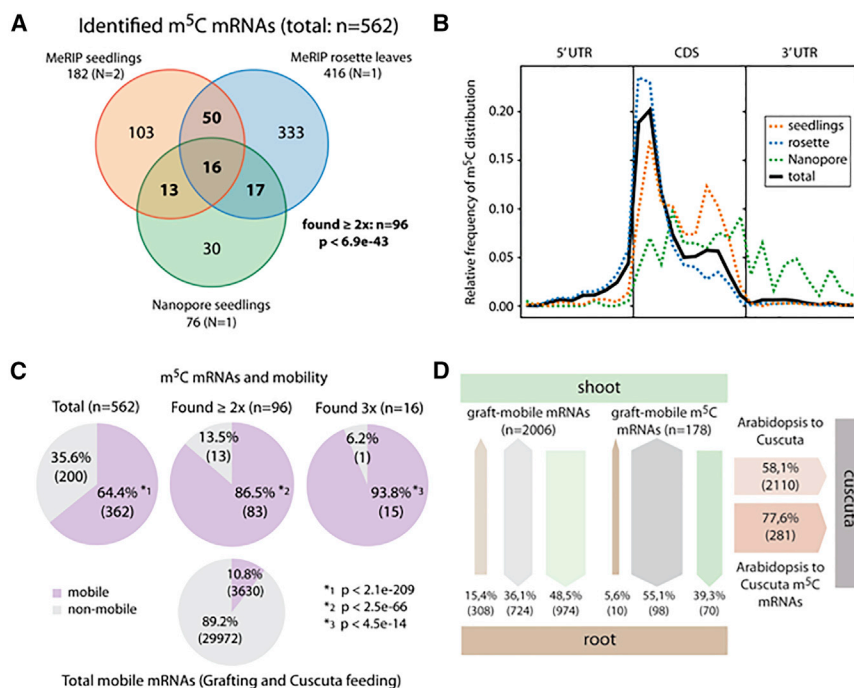


**Figure 1. Identified m<sup>5</sup>C mRNAs and Enrichment of Graft-Mobile Transcripts**

(A) Venn diagram showing the overlap of the three independent datasets of m<sup>5</sup>C transcripts identified via MeRIP of *Arabidopsis thaliana* (ecotype Col-0) seedlings and rosette leaves and via Nanopore sequencing of seedling RNA samples. The total number of m<sup>5</sup>C transcripts (n = 562) overlaps significantly between MeRIP seedlings and MeRIP rosette-leaf datasets (n = 66,  $p < 6.4e-79$ ), between MeRIP seedlings and Nanopore seedlings (n = 29,  $p < 1.3e-46$ ), and between MeRIP rosette leaves and Nanopore seedlings (n = 33,  $p < 7.0e-43$ ), as calculated with exact hypergeometric probability using a total number of 33,602 genes in the genome as background. Ninety-six transcripts are found in at least two datasets, and 16 are common among all three.

(B) Relative frequency of m<sup>5</sup>C distribution along relative transcript lengths. The dashed lines represent their distribution according to the individual datasets. The black line represents the average of all three distributions.

(C) Ratio of mobile transcripts in the m<sup>5</sup>C population. The bottom pie shows the percentage of mobile transcripts identified previously [1] in the total of *Arabidopsis* transcripts. Mobile

transcripts are significantly enriched in the datasets of total m<sup>5</sup>C mRNAs (64.4%,  $p < 2.1e-209$ ), found at least twice (86.5%,  $p < 2.5e-66$ ), and found three times (93.8%,  $p < 4.5e-14$ ).

(D) Directionality of all graft-mobile transcripts in *Arabidopsis* (left) as previously described [1] and in the subset of total m<sup>5</sup>C transcripts (right). On the right, mobile transcripts that moved from *Arabidopsis* to *Cuscuta*, both the total amount (top arrow) and the m<sup>5</sup>C subset (bottom arrow), are shown. There is a significant change of the distribution of the mobile transcripts among the different groups: root-to-shoot and shoot-to-root appear under-represented in the m<sup>5</sup>C transcripts ( $p < 1.9e-05$  and  $p < 0.0023$ , respectively), whereas bidirectional and *Arabidopsis*-to-*Cuscuta* graft-mobile transcripts are overrepresented ( $p < 3.0e-08$  and  $p < 1.3e-16$ , respectively). See also Figures S1 and S2 and Data S1.

Mobile non-coding RNAs, such as tRNAs, first identified in pumpkin phloem exudate, are biased in their quantity and identity. For example, *tRNA-Met* (ATG), *tRNA-Pro* (AGG), *tRNA-Gly* (GGA), and *tRNA-Asp* (GAC) are highly abundant whereas *tRNA-Ile* (TAT)—although expressed highly in leaves—could not be detected in phloem exudates [23]. Non-mobile transcripts such as *GUS* gain mobility if fused to *tRNA-Gly* or *tRNA-Met* but not with *tRNA-Ile* [16]. This correlates with specific m<sup>5</sup>C modifications found in *Arabidopsis* tRNAs such as *tRNA-Gly*, which is methylated at many cytosines, whereas cytosines of *tRNA-Ile* appear to be either scarcely or not at all methylated [24]. Such base modifications have the potential to alter transcript stability, functionality, structure, and consequently, interaction with cellular factors [25–27] that could mediate transcript transport to distant tissues. Given that phloem tRNAs and graft-mobile mRNAs harboring TLS motifs are likely to be targeted by the RNA m<sup>5</sup>C methyltransferases *DNMT2/TRDMT1* and *NSUN2B/TRM4B* [24, 28–31], we asked whether m<sup>5</sup>C methylation plays a role in mRNA transport to distant cells via the phloem.

## RESULTS

### A Significant Number of Mobile mRNAs Harbor Methylated Cytosines

We first performed RNA immunoprecipitation using an antibody against m<sup>5</sup>C [29] followed by sequencing (MeRIP-seq) to identify

mRNAs that carry methylated cytosines. Two mRNA populations were examined, one from *Arabidopsis* seedlings harvested 10 days after germination and another from rosette leaves harvested from adult bolting plants. We identified in these two populations 182 and 416 m<sup>5</sup>C methylated mRNA transcripts, respectively. A third dataset of 76 m<sup>5</sup>C mRNAs was obtained by Nanopore methylation sequencing of RNA samples from seedlings (Data S1A). In total, 562 distinct m<sup>5</sup>C mRNAs were identified via these combined approaches. Despite the different developmental stages and methods used for identifying m<sup>5</sup>C mRNAs, there is a highly significant overlap among the three datasets with 96 mRNAs found in at least two of them and 16 mRNAs found in all three datasets (Figure 1A). The relative distribution of the m<sup>5</sup>C positions along the length-normalized UTR and coding sequence (CDS) regions reveals a strong m<sup>5</sup>C enrichment in the CDS region with a peak at the translational start site of the CDS and a secondary, less pronounced peak toward the 3' end of the CDS (Figure 1B; Figure S1A). To evaluate the number of mobile transcripts harboring m<sup>5</sup>C, we compared the m<sup>5</sup>C mRNA population with the mobile (n = 3,630) versus non-mobile assigned (n = 29,972) transcripts that were identified by SNPs in hetero-grafted *Arabidopsis thaliana* Col-0 and *Ped* ecotypes and in *Cuscuta reflexa* feeding on *Arabidopsis thaliana* accession C24 [1]. A highly significant number of the 562 m<sup>5</sup>C transcripts were previously assigned as mobile mRNA (n = 362, 64.4%,  $p < 2.1e-209$ ), indicating a potential relationship

between detected m<sup>5</sup>C mRNA modifications and transcript mobility (Figure 1C; Figure S1B). These 362 m<sup>5</sup>C-modified and mobile transcripts include *TCTP1* and *CAT3* transcripts, which were individually confirmed to be graft-transmissible [1]. Notably, considering m<sup>5</sup>C mRNAs identified at least twice (n = 96) or in all three datasets (n = 16) (Data S1C and S1D), the proportion of mobile transcripts increases to 86.5% (n = 83, p < 2.5e−66) and to 93.8% (n = 15, p < 4.5e−14), respectively (Figure 1C). This finding supports the hypothesis that m<sup>5</sup>C contributes to transcript mobility.

The methylated- and mobile-assigned transcripts were further analyzed based on their transport directionality (shoot-to-root, root-to-shoot, or both) [1] (Figure 1D). The relative distribution of the m<sup>5</sup>C mRNA transport directionality differs from that of all the mobile 3,630 mRNAs showing a significant enrichment in bi-directional graft-mobile transcripts (p < 3.0e−08) and accordingly, a decrease in the shoot-to-root and root-to-shoot direction (p < 0.0023 and p < 1.9e−05, respectively). *Arabidopsis* to *Cuscuta* mobile transcripts are also enriched among the m<sup>5</sup>C mRNAs (p < 1.3e−16).

Recently, Cui et al. [31] used a similar but less conservative analysis to determine the m<sup>5</sup>C transcriptome of *Arabidopsis* seedlings (n = 4,465), which overlaps significantly with the 182 methylated transcripts found in our MeRIP seedling experiments (n = 105, 58%, p < 2.9e−45). Also, this reported m<sup>5</sup>C transcriptome significantly overlaps with all 562 m<sup>5</sup>C transcripts found in our analysis (n = 259, 46%, p < 1.7e−81) (Data S1E) and with the 3,630 reported mobile transcripts [1] (n = 1,493, 33.4%, p < 5.0e−324). Notably, enrichment of mobile transcripts increases if we consider the top 500 methylated mRNA candidates according to their p value (232 transcripts or 46.4% overlap, p < 6.4e−92) (Data S1E).

Similar to a previously performed analysis for TLS motifs enriched in mobile *Arabidopsis* mRNAs [16], we scanned the sequences of our identified 562 m<sup>5</sup>C mRNAs for TLS [32]. This revealed that 12.1% of the methylated population (n = 68 of 562) harbors a potential TLS motif, which is significantly increased (p < 0.01) compared to all transcripts from annotated genes (9.36%; n = 3,145 of 33,602). However, this seems to be a weak relation as the co-occurrence of mRNA cytosine methylation and TLS motifs is comparable to the reported significant occurrence of TLS motifs in the mobile transcript population of approximately 12% [16].

We next scanned for the PTB sequence motif proposed to trigger mobility of transcripts [22] by taking all sequences enriched for methylation (2,325 unique sequence windows of 25 nt length; see STAR Methods) and performing a motif search using DREME [33]. This revealed five significantly enriched motifs of which two were identified previously in connection to RNA cytosine methylation (CC[AUG]CC[AG]) and (C[UA]UCUUC) [31] (Figure S1C). The latter seems to resemble a previously reported PTB—UUCUCUCUCUU—sequence motif [22] that we termed PTB-like. The first methylation motif (CC[AUG]CC[AG]) can be found in 403 methylated 25 nt windows belonging to 182 transcripts. 64.8% (118 of 182) of those are mobile, reflecting approximately the mobility rate of all methylated transcripts (64.4%, 362 of 562). The PTB-like methylation motif (C[UA]UCUUC) is found in 86 windows belonging to 82 transcripts, and interestingly, 61 of those transcripts are reported to be

mobile (74.4%), which is a significant enrichment (p < 0.05) compared to the mobility rate of all methylated transcripts. Transcripts carrying both motifs (n = 39) show the same enrichment for mobility as the ones containing only the PTB-like motif (74.4%, 29 of 39). As with the TLS motif, the PTB-like motif is found in a relatively small number of methylated and mobile transcripts and might play a specific role in facilitating transport of a subset of transcripts such as *GAI* or *StBEL5*, that are suggested to regulate growth of distant tissues [18, 20–22].

To address whether the abundance of m<sup>5</sup>C tagged transcripts is significantly different from the whole transcriptome, we compared the relative levels of MeRIP-enriched mRNAs to all mRNAs found in MeRIP control samples. This analysis revealed that highly abundant transcripts were enriched in MeRIP samples and that the chance of finding m<sup>5</sup>C transcripts does increase with the expression level of the corresponding genes (Figure S2A).

The m<sup>5</sup>C transcripts were also analyzed for their stability according to the half-life data available for ~12,000 mRNAs published by Narsai et al. [34]. The analysis showed that mRNAs undergoing m<sup>5</sup>C methylation are significantly more stable compared to non-methylated RNAs (p < 1.3e−16; Figure S2B). Methylated and mobile transcripts, however, were not significantly more stable than the total m<sup>5</sup>C mRNAs identified, suggesting that mobile mRNAs are not significantly different in their half-life than any other methylated transcript. Here, it should be noted that due to the MeRIP protocol and parameters used in the analysis to call enriched peaks of transcripts (see STAR Methods), there is an increased likelihood of identifying more stable and abundant transcripts. Thus, we could not have easily found very lowly expressed or unstable transcripts, which would allow for a more thorough analysis of the effect of m<sup>5</sup>C methylation on mRNA abundance and mobility.

To further evaluate whether m<sup>5</sup>C modification relates to mRNA movement in plants, we chose two transcripts from the 362 mobile m<sup>5</sup>C-modified mRNAs that were found twice in our m<sup>5</sup>C databases and lack a predicted TLS motif (Data S1). The first one is *HSC70.1* (TAIR# AT5G02500) harboring PTB-like motifs, and the second is *TCTP1* (TAIR# AT3G16640) lacking a PTB-like motif.

### ***TCTP1* Transcript Mobility Depends on Specific mRNA Sequences and Is Not Transported in m<sup>5</sup>C Methylation-Deficient *dnmt2 nsun2b* Mutants**

We noted in previous experiments that, in contrast with *YFP* transcript, a full-length *Arabidopsis thaliana TCTP1* ORF (open reading frame) transcript fused to *YFP* moves from above ground tissue (shoot, scion) to roots (root stock) in hypocotyl grafted plants [1]. To address a possible function of m<sup>5</sup>C in mRNA transport, we used a 35S *CaMV* promoter to express full-length *TCTP1* ORF and deletion variants thereof and *TCTP1M* with alternative codon usage fused to *YFP* (*YFP-TCTP1M*) in *Arabidopsis* wild type (Col-0) and the mRNA methylation-deficient *dnmt2 (trdmt1) nsun2b (trm4b)* double mutant [24] (Figure 2A; Figures S2C, S3, and S4A–S4C; Data S2A–S2F). These *YFP-TCTP1* fusions include or exclude identified *TCTP1* m<sup>5</sup>C modification sites (*YFP-TCTP1Δ3'*, *YFP-TCTP1Δ5'*, *YFP-TCTP1Δ5'Δ3'*, *YFP-TCTP1ΔA*, and *YFP-TCTP1M*) and predicted stable 3' and 5' folding structures according to minimal free energy RNA folding (MFE) [35, 36] and co-transcriptional



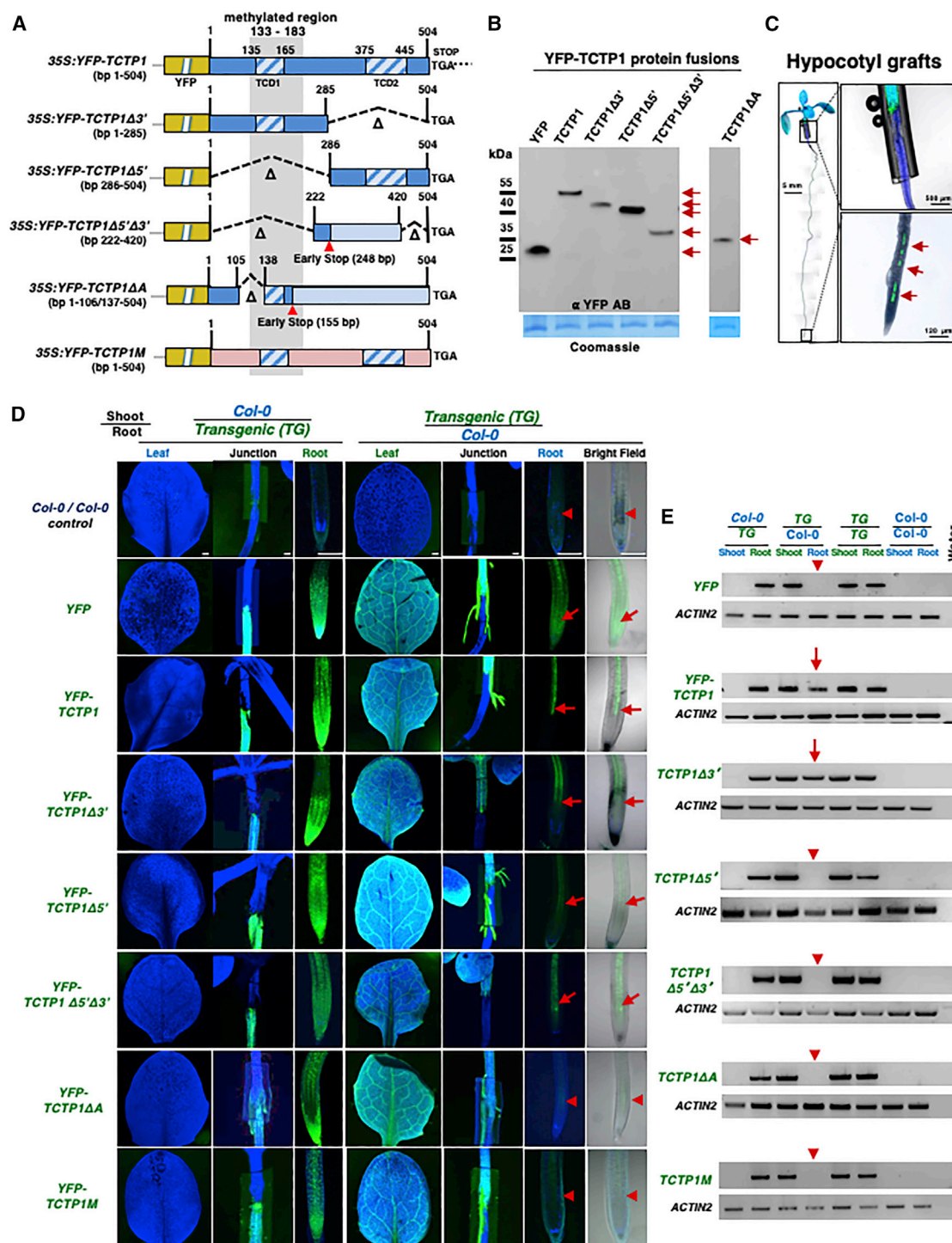


**Figure 2. Mobility of YFP-TCTP Fusion Constructs in Hypocotyl Grafted Arabidopsis**

(A) Schematic drawing of *TCTP1* (504 bases, 168 amino acids) YFP fusion and deletion constructs used in the study. Gray background (bases 133–183) indicates the MeRIP-identified m<sup>3</sup>C-edited region in *TCTP1* ORF. YFP-TCTP1Δ3', bases 1–285; YFP-TCTP1Δ5', bases 286–504; YFP-TCTP1Δ5'Δ3', bases 222–420; YFP-TCTP1ΔA, bases 1–106/137–504. TCD1 (bases 135–165) and TCD2 (bases 375–445) indicate conserved *TCTP1* domains. Red arrows indicate early stop codons due to a frameshift (Data S2), and blue indicates predicted ORF sequences.

(B) Western blot detection of YFP fusion proteins produced in 2-week-old transgenic *Arabidopsis* (Col-0) seedlings by GFP/YFP-specific antibodies. Calculated protein sizes including linker sequences are: YFP 31 kDa, YFP-TCTP1 53.5 kDa, YFP-TCTP1Δ3' 49 kDa, YFP-TCTP1Δ5' 47.5 kDa, YFP-TCTP1Δ5'Δ3' 38 kDa, YFP-TCTP1ΔA 39 kDa. Red arrows mark apparent sizes of the YFP fusions. Lower panel shows the loading control.

(legend continued on next page)

folding (Co-Fold) predictions [37] (Figure S2C). We first determined whether the various YFP-TCTP1 fusion constructs are stably expressed (Figure 2B; Figures S3 and S4A–S4C) and whether the intracellular protein localization is altered between the transformed wild-type and *dnmt2 nsun2b* lines (Figures S4A–S4C). To address this, we compared the subcellular distribution of the YFP-TCTP1 fusion proteins produced in wild-type and *dnmt2 nsun2b* plants by confocal laser scanning microscope (CLSM) imaging. This revealed that the localization of all YFP-TCTP1 protein fusions did not change between wild-type and *dnmt2 nsun2b* mutant plants. In contrast to both YFP-TCTP1 and YFP-TCTP1M, all YFP-TCTP1 deletion proteins showed a change in their subcellular distribution. Both full-length YFP-TCTP1 fusion proteins were barely detectable in nuclei and seemed to accumulate at nuclear envelopes, whereas the C-terminal truncated YFP-TCTP1 fusions appeared equally distributed between cytosol and nucleus (Figures S3 and S4A–S4C).

To study the transport of the YFP-TCTP1 protein and YFP-TCTP1 transcripts and variants thereof, we grafted YFP-TCTP1 lines (TG) with wild type (Col-0) (Figures 2C and 2D). As previously shown in grafting experiments [1], CLSM and RT-PCR assays revealed that both full-length YFP-TCTP1 protein and YFP-TCTP1 transcript produced in transgenic wild-type shoots are present in grafted wild-type roots (Figures 2D and 2E).

Next, we tested the mobility of the proteins and transcripts produced by the TCTP1 variants in grafted plants. Both TCTP1Δ3' and TCTP1Δ5' produce truncated proteins from transcripts predicted to retain their RNA folding structures detected in their respective 5' and 3' ORF regions. The YFP-TCTP1Δ5'Δ3' is lacking the major folding domains predicted in both 5' and 3' TCTP1 halves, YFP-TCTP1ΔA lacks part of the identified methylation region of TCTP1, and YFP-TCTP1M shows a changed folding structure in all regions (Figure 2A; Figure S2C). Both YFP-TCTP1Δ3' and YFP-TCTP1Δ5'Δ3' proteins were easily detected in grafted wild-type roots (Figure 2D). However, YFP-TCTP1Δ5' and YFP-TCTP1ΔA, which are smaller than YFP-TCTP1Δ3' fusion proteins (Data S2B), and YFP-TCTP1M, which has the same protein sequence and subcellular distribution as YFP-TCTP1 (Figures S3 and S4A–S4C; Data S2F and S2G), were barely or not detectable in grafted wild-type roots. This suggests that these TCTP1 variants are not capable to efficiently diffuse from shoot to root in grafted plants and that the YFP-TCTP1 presence in the grafted wild-type roots depends on TCTP1 RNA sequences.

In contrast with the YFP-TCTP1Δ3' deletion, none of the other TCTP1 deletion constructs missing the identified methylated 5' region stretching from base +133 to +183 (YFP-TCTP1Δ5',

YFP-TCTP1Δ5'Δ3', and YFP-TCTP1ΔA) and the YFP-TCTP1M with altered RNA structure were detected in RT-PCR assays on grafted wild-type root RNA samples (Figure 2E). These combined results indicate that the 5' and 3' TCTP1 UTRs, both harboring potential PTB motifs suggested to mediate transcript mobility [22], are dispensable for TCTP1 mobility. It seems that the TCTP1 5' ORF stretching from the start codon base +1 to base +285 contains the RNA sequence necessary and sufficient to cause YFP mobility. This result, together with the finding that the YFP-TCTP1ΔA transcript missing part of the m<sup>5</sup>C methylated region lacks transport activity over graft junctions, indicates that m<sup>5</sup>C modifications facilitate transcript mobility.

To address whether YFP-TCTP1 protein or YFP-TCTP1 transcript mobility depends on m<sup>5</sup>C RNA methylation, we used mutant *Arabidopsis thaliana* ecotype Col-0 plants lacking DNMT2 and NSUN2B methyltransferase activity. To this end, we grafted *dnmt2 nsun2b* mutant root stocks with wild-type (Col-0) or *dnmt2 nsun2b* mutant scions expressing YFP-TCTP1 or YFP-TCTP1Δ3' (>2 independent transgenic lines, each n > 10). In contrast with transgenic wild-type scion/*dnmt2 nsun2b* root-stock grafts (Figure 3A), YFP-TCTP1 and TCTP1Δ3' fusion proteins expressed in *dnmt2 nsun2b* shoots were barely or not detectable in roots of transgenic *dnmt2 nsun2b/dnmt2 nsun2b* grafts (Figure 3A). To inspect whether the mobile YFP-TCTP1 and YFP-TCTP1Δ3' transcripts move from *dnmt2 nsun2b* shoots to *dnmt2 nsun2b* roots, we performed RT-PCR assays on shoot (positive control) and root samples from the grafted plants (Figure 3B). YFP-TCTP1 and YFP-TCTP1Δ3' transcripts were detected in transgenic *dnmt2 nsun2b* and wild-type shoot and in wild-type/*dnmt2 nsun2b* root, but not in *dnmt2 nsun2b/dnmt2 nsun2b* root samples (Figures 3B and 3C). Notably, in *dnmt2 nsun2b* roots grafted with YFP-TCTP1 or YFP-TCTP1Δ3' wild-type (Col-0) scions, we detected relatively low levels of fluorescent fusion proteins (Figure 3A), which correlates with relatively low occurrence of YFP-TCTP1 or YFP-TCTP1Δ3' transcripts in these roots (Figure 3B). Therefore, lack of DNMT2 and NSUN2B mRNA methylation activity diminishes TCTP1 transport to roots. Absence of YFP-TCTP1 transcript movement across graft junctions in *dnmt2 nsun2b* mutants seems not to be a result of lower transcript levels as both transgenic and endogenous TCTP1 transcript levels were comparably high in *dnmt2 nsun2b* and in Col-0 plants according to qRT-PCR assays (Figures 3C and 3D; Figure S3E).

A previous study suggested that m<sup>5</sup>C mRNAs display increased stability [38]. Thus, we next asked whether cytosine methylation by the RNA methyltransferases DNMT2 and NSUN2B affects decay of TCTP1 by measuring the mRNA levels

(C) Representative confocal laser scanning microscope (CLSM) image of a representative hypocotyl-grafted YFP-TCTP1 (shoot)/Col-0 (root) plant 10 days after grafting (DAG) as used in the study. Note that a YFP-TCTP1 (green) fluorescent signal is present in the wild-type root (red arrow).

(D) YFP fluorescent signal detected by CLSM in leaves, graft junctions, and primary root tips of grafted YFP-TCTP1, YFP-TCTP1Δ3', YFP-TCTP1Δ5', YFP-TCTP1Δ5'Δ3', YFP-TCTP1ΔA/wild-type (Col-0) plants. Blue indicates auto-fluorescent background, red arrows indicate YFP signal detected, and red arrowheads indicate YFP signal not or barely detected in grafted transgenic (scion)/Col-0 (root stock) root tips. Three independent lines (each n > 30 plants) were used for each graft combination, and each shows a similar distribution of the YFP signal. Scale bar: 200 μm.

(E) RT-PCR detection of YFP-TCTP1 fusion constructs on root and shoot RNA samples of grafted plants. RNA from grafted plants (n > 6) was pooled and tested by RT-PCR (45 PCR cycles) for the presence of YFP, YFP-TCTP1, YFP-TCTP1Δ3', YFP-TCTP1Δ5', YFP-TCTP1Δ5'Δ3', and YFP-TCTP1ΔA fusion transcripts in shoots and roots. Red arrows indicate the specific presence YFP-TCTP1 bands in Col-0 samples, and red arrowheads indicate the absence of YFP-TCTP1 bands in Col-0 samples of grafted plants. Note that absence of TCTP1 RNA was confirmed by 50 PCR cycles.

See also Figures S2 and S3.

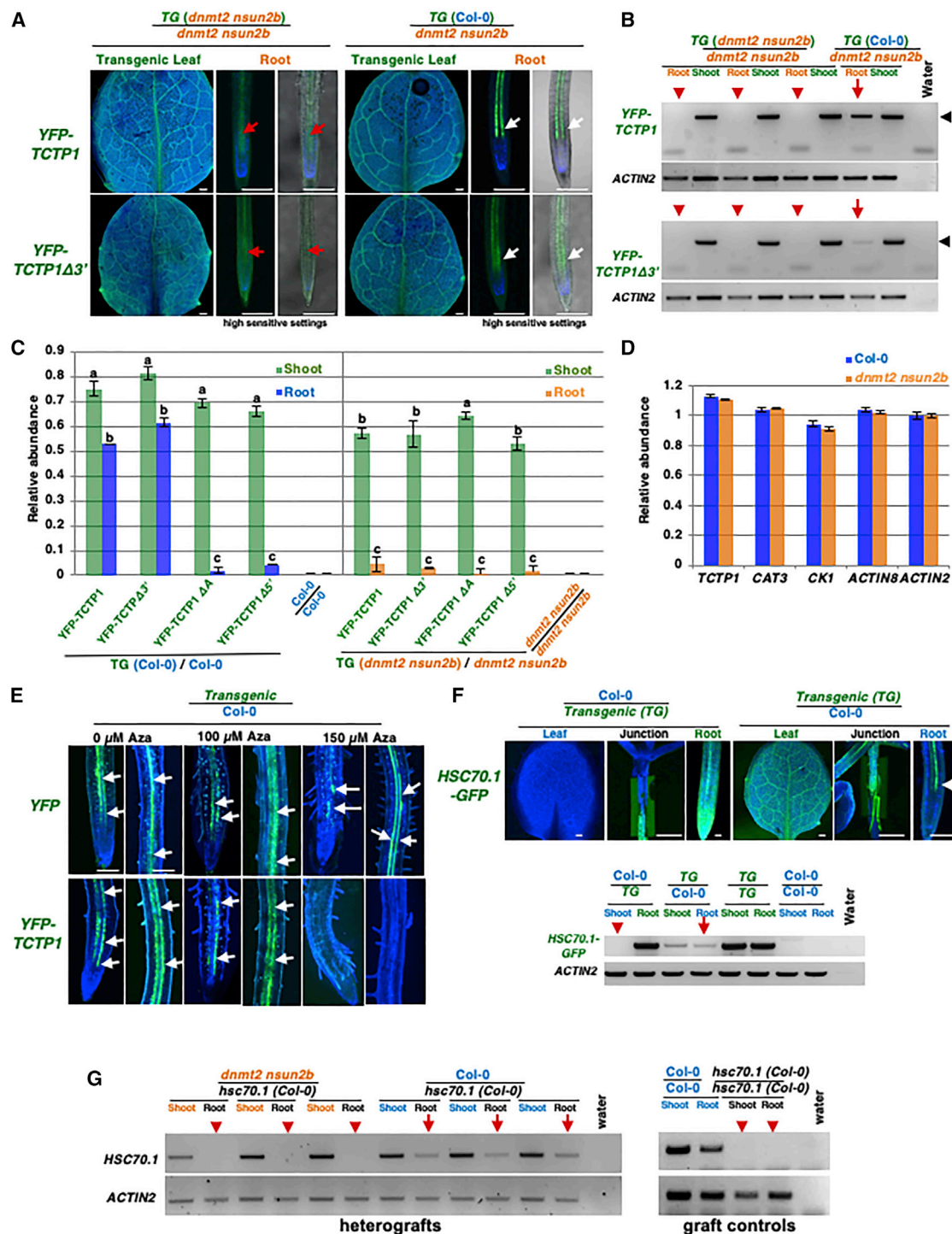


**Figure 3. YFP-TCTP1 Transcript Mobility in Hypocotyl-Grafted *dnmt2 nsun2b* Double Mutants**

(A) YFP fluorescent signals in leaves, graft junction, and primary root tips detected in YFP-TCTP1 (*dnmt2 nsun2b*)/*dnmt2 nsun2b* and YFP-TCTP1 (Col-0)/*dnmt2 nsun2b* grafted plants. Blue indicates auto-fluorescence, red arrows indicate very weak or no YFP fluorescence, and white arrows indicate high YFP fluorescence detected in *dnmt2 nsun2b* root tips with high-sensitive confocal settings. Two independent transgenic lines were used for each graft combination all showing similar YFP distribution patterns. Scale bar: 200 μm.

(B) RT-PCR assays on root and shoot RNA samples from grafted plants. Plant tissues from grafted seedlings (>7) were pooled and tested for the presence of YFP-TCTP1 and YFP-TCTP1Δ3' fusion transcripts in grafted tissues. Red arrows indicate the presence of YFP-TCTP1 fusion transcripts, red arrowheads indicate the absence of fusion transcripts, and black arrowhead indicates expected PCR product. Note that lower, faint bands are primers used in the PCR reaction.

(legend continued on next page)



in seedlings of 14-day-old wild-type and *dnmt2 nsun2b* plants treated with the transcription inhibitor actinomycin D. We measured the transcript levels of m<sup>5</sup>C-modified mobile *TCTP1*, *CAT3*, and *CK1* transcripts [1, 16], non-mobile assigned m<sup>5</sup>C-modified *ACTIN8*, and non-m<sup>5</sup>C-modified *ACTIN2* in *dnmt2 nsun2b* and Col-0 plants by qRT-PCR. For these transcripts, no significant difference in their abundance was found in the *dnmt2 nsun2b* mutant compared with wild type ( $p > 0.3$ ) (Figure 3D). Also, both *TCTP1* and *ACTIN8* showed no significant difference in their RNA stability in *dnmt2 nsun2b* versus wild-type plants from 12 to 24 h after actinomycin D treatment (Figure 3D). Similarly, the non-m<sup>5</sup>C-modified transcript *TUBULIN2* (*TUB2*) displayed unchanged RNA stability (Figure S4D). This suggests that altered abundance of transcripts is not the reason for the observed lack of their mobility.

### Inhibition of Cytosine Methylation Inhibits YFP-TCTP1 Transcript but Not YFP Protein Diffusion

To additionally confirm that methylation activity is necessary for transcript mobility, we grew YFP or YFP-*TCTP1* transgenic (shoot)/Col-0 wild-type (root stock) grafted plants in liquid MS supplemented with no (control), medium (100  $\mu$ M), and high (150  $\mu$ M) concentrations of 5-Azacytidine (Aza) (Figure 3E). Aza acts as a pleiotropic inhibitor of m<sup>5</sup>C modification [28], and we expected that it affects movement of *TCTP1* mRNA similar to that seen in *dnmt2 nsun2b* mutants. Presence of 150  $\mu$ M Aza did not interfere with phloem-mediated diffusion of YFP protein over graft junctions as indicated by detected yellow fluorescence in the phloem associated cells of grafted wild-type roots (Figure 3E). However, in grafted YFP-*TCTP1*/Col-0 plants incubated with medium (100  $\mu$ M) or high (150  $\mu$ M) concentration of Aza, YFP-*TCTP1* protein was weakly or not detected in wild-type roots ( $n > 10$ ) (Figure 3E), implying that *TCTP1* transcript mobility and not *TCTP1* protein mobility depends on m<sup>5</sup>C methylation. Considering that diffusion of YFP alone to wild-type roots is not hindered by Aza treatment and that no YFP-*TCTP1* fluorescence can be detected in roots of 150  $\mu$ M Aza treated YFP-*TCTP1*/wild-type grafted plants, this result suggests that YFP-*TCTP1* transcript is translated to functional protein in receiving root cells. Thus, the presence of YFP-*TCTP1* fluorescence detected in wild-type roots of grafted plants is a result of transcript mobility

rather than phloem-mediated shoot-to-root YFP-*TCTP1* protein transfer.

### Mobility of Endogenously Produced HSC70.1 Transcript Depends on Cytosine Methylation

First, to evaluate whether transcripts transported over graft junctions might depend on their expression from the 35S *CaMV* promoter, we used transgenic lines expressing *HSC70.1-GFP* from the *UBIQUITIN 10* (*UBQ10*) promoter and grafted these with Col-0 wild type. Here, as seen with 35S::YFP-*TCTP1*/wild-type grafted plants (Figure 2), the *HSC70.1-GFP* fusion protein and its transcript were detected in *HSC70.1-GFP*/wild-type roots but not in aboveground wild-type tissue in wild-type/*HSC70.1-GFP* grafted plants (Figure 3F). Thus, transcript mobility is independent of the promoter used to express the transgene. We next asked whether endogenously produced *HSC70.1* transcript is also graft mobile and whether its mobility depends on m<sup>5</sup>C methylation. To address this, we grafted *hsc70.1* mutant with wild-type (Col-0) or *dnmt2 nsun2b* double-mutant plants (Figure 3G). In according controls (wild-type shoot grafted with *hsc70.1* roots), the *HSC70.1* transcript was detected in root samples, corroborating that endogenous *HSC70.1* is mobile when produced in wild-type plants (Figure 3G). In contrast with wild-type controls, absence of an *HSC70.1*-specific RT-PCR band in *dnmt2 nsun2b/hsc70.1* mutant root RNA samples indicates a lack of mobility of the endogenous *HSC70.1* transcript in *dnmt2 nsun2b* mutants. In summary, these data suggest that mobility of the endogenously produced *HSC70.1* transcript depends on m<sup>5</sup>C modification.

### YFP-TCTP1 and YFP Are Differentially Distributed in Root Tissues

Pumpkin and *Brassica napus* (rapeseed) phloem sap contain *TCTP1* protein suggesting that not only *TCTP1* transcript but also the relatively small protein of 18.9 kDa has the potential to diffuse like YFP via intercellular plasmodesmatal channels into the phloem vasculature and over long distances into the root tip [17, 39, 40]. However, compared with YFP, the distribution of YFP-*TCTP1* fusion appeared to be very different in the vasculature and root tip (Figure 2D), raising the question into which cell types the protein or transcript is transferred. To address this, we analyzed the distribution of YFP-*TCTP1* protein by

(C) qRT-PCR to measure relative transcript levels of mobile and non-mobile YFP-*TCTP1* fusion transcripts, adjusted according to reference transcript *UBIQUITIN10* thresholds. YFP-*TCTP1* fusions in grafted transgenic *dnmt2 nsun2b* shoot and *dnmt2 nsun2b* root (three biological, three technical replicates). TG (Col-0), transgenics in Col-0 background; TG (*dnmt2 nsun2b*), transgenics in *dnmt2 nsun2b*. YFP-*TCTP1* values serve as a reference for *TCTP1* mobility ( $p$  values are indicated by a, b, and c.  $ab < 0.1$ ;  $ac < 0.001$ ;  $bc < 0.001$ ).

(D) qRT-PCR assays measuring relative transcript levels of mobile and/or methylated transcripts in *dnmt2 nsun2b* compared to Col-0 controls. No significant ( $p > 0.05$ ) difference of expression/abundance of transcripts was observed. Values are mean  $\pm$  SD from three independent experiments.

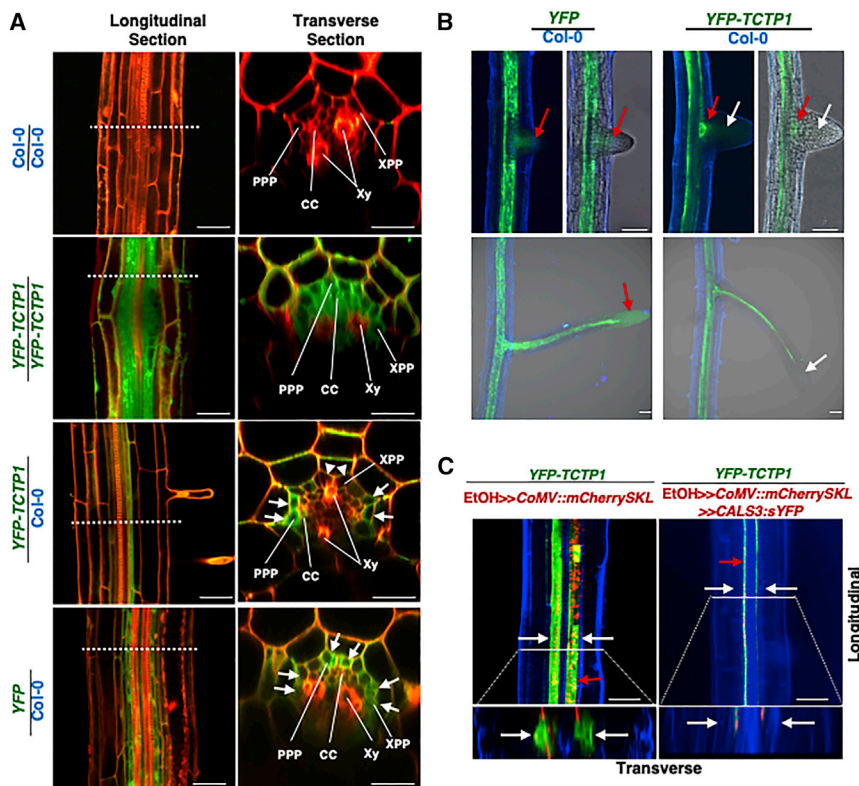
(E) YFP fluorescent signals in primary root tips detected in YFP-*TCTP1* (Col-0)/Col-0 grafted plant treated with 0  $\mu$ M (control), 100  $\mu$ M, or 150  $\mu$ M Azacytidine (Aza). White arrows indicate YFP-specific fluorescence signals. Scale bar: 100  $\mu$ m.

(F) Mobility of the *HSC70.1-GFP* fusion and endogenous *HSC70.1* transcript. Upper panel: GFP fluorescent signals detected by CLSM in leaves, graft junctions, and primary root tips of *HSC70.1-GFP* lines grafted with Col-0 plants. Blue indicates auto-fluorescence, and white arrows indicate GFP signals detected in wild-type root tips of grafted plants. Three independent lines (each  $n > 30$  plants) were used for each graft combination. All showed similar distribution of the GFP signal. Scale bar: 200  $\mu$ m. Lower panel shows *HSC70.1-GFP*-specific RT-PCR assays on root and shoot RNA samples of grafted plants. RNA from shoots and roots (each a pool of  $n > 6$ ) were submitted to RT-PCR (45 PCR cycles). Red arrows indicate the presence of *HSC70.1-GFP* mRNA in Col-0 samples, and red arrowheads indicate the absence of *HSC70.1-GFP* mRNA in Col-0 samples.

(G) RT-PCR assays to detect endogenous *HSC70.1* in root and shoot of grafted *dnmt2 nsun2b* and *hsc70.1* plants. Red arrows indicate the presence of *HSC70.1* in *hsc70.1* mutant root samples of Col-0/*hsc70.1* grafted plants, and arrowheads indicate the absence of *HSC70.1*-specific bands in *hsc70.1* mutant root samples of *dnmt2 nsun2b/hsc70.1* grafted plants.

See also Figures S3 and S4.





mCherrySKL (red punctae) and YFP-TCTP1 (green) in phloem-associated cells. White arrows indicate the stele width where mCherrySKL-tagged peroxisomes (red) and YFP-TCTP1 fluorescence (green) are not detected in grafted transgenic roots expressing CALS3::sYFP. Note that the EtOH-inducible CoMV promoter drives specific expression in CC and that the fluorescence emission of YFP fused to CALS3 is shifted by approximately  $-20$  nm (named sYFP), and thus CALS3-sYFP is not detected by the CLSM settings used (see STAR Methods and Figure S5). Scale bar:  $100\ \mu\text{m}$ . See also Figure S5.

high-resolution CLSM on wild-type roots grafted with YFP-TCTP1 shoots. In grafted non-transgenic wild-type roots, YFP-TCTP1 specific fluorescent signals were detected in cells associated to the phloem vasculature (Figures 4A and 4B). In contrast with YFP alone, YFP-TCTP1 was not present in the root tip and appeared mainly in cells forming the phloem in the root differentiation zone (Figures 2D and 4B). To reveal the cell types in which YFP or YFP-TCTP1 is detected, we performed a series of high-resolution longitudinal and transverse CLSM images. YFP appeared to be unloaded to all vascular bundle (stele) cells including the endodermis, pericycle, and all parenchyma cells. In contrast, YFP-TCTP1 fluorescence appeared more restricted to the phloem parenchyma, was relatively high in phloem pole pericycle (PPP) cells, appeared weaker in companion cells (CCs), was barely detectable in endodermal cells connected to the PPP cells, and was not detected in other stele cells such as xylem pole pericycle (XPP) cell files adjacent to the xylem (Figure 4A). Control grafts with YFP-TCTP1-expressing roots indicate that the observed YFP-TCTP1 distribution in wild-type roots was not a result of protein or transcript instability in endodermis—and phloem/xylem—associated parenchyma cells as the fusion protein appeared equally in all these cell types. Similarly, differences in unloading of YFP and YFP-TCTP1 were evident by the absence of YFP-TCTP1 in the root tip and regions where lateral root primordia form. As previously reported [15, 17], YFP diffuses into primary and lateral root tips (Figure 4B).

YFP-TCTP1, however, appears to be defined to phloem-associated cells in the main and lateral root tips and is detected in a narrow central region at sites of emerging lateral roots (Figure 4B).

Delivery of YFP-TCTP1 into PPP cells would be consistent with the proposed notion that these cells are the main repositories for phloem-delivered macromolecules [15]. To test this, we grafted YFP-TCTP1 plants with root stocks co-expressing a green fluorescent fusion of CALLOSE SYNTHASE-LIKE 3 (CALS3) and Cherry-SKL (peroxisomal marker diffusing between cells) in CC cells from an EtOH-inducible CoMV promoter specifically active in CC (Figure 4C). High CALS3 activity in CC induces callose deposition at plasmodesmata (PD) and blocks diffusion of macromolecules via PD [41]. In ethanol-incubated plants closure of PD induced by CoMV >> CALS3 is indicated by a lack of Cherry-SKL diffusion from CCs to phloem neighboring cells via PD (Figure 4C; Figures S5A and S5B). Interestingly, callose-induced blockage of PD in CoMV >> CALS3 roots constricts the presence of YFP-TCTP1 fluorescence to CC suggesting that YFP-TCTP1 transcript transport to PPP cells depends on functional PD in CC connecting neighboring cells.

#### Mobile TCTP1 Transcript Promotes Root Growth

TCTP1 is an important growth regulator in *Arabidopsis* [42]. We noticed that transgenic plants expressing YFP-TCTP1 display enhanced rosette growth (Figure S5C) suggesting that the fusion protein acts similar to the endogenous produced TCTP1 as a growth factor. To test whether YFP-TCTP1 mobility is necessary

#### Figure 4. Different Distribution of YFP and YFP-TCTP1 Protein in Grafted Wild-Type Root Stocks

CLSM images of wild-type roots grafted with YFP and YFP-TCTP1-expressing plants.

(A) Longitudinal and transverse CLSM images of roots formed on auto- and hetero-grafted YFP-TCTP1, YFP, and Col-0 plants. Note that in wild-type (Col-0) roots, YFP is detected in phloem pole pericycle (PPP) cells, companion cells (CCs), and xylem pole pericycle (XPP) cells. YFP-TCTP1 is detected in PPP cells and CCs but not in XPPs. White arrows indicate the presence of YFP fluorescence, white arrowheads indicate the absence of YFP fluorescence in XPPs, red indicates propidium-iodide-stained cell-wall material, and green indicates YFP fluorescence. Xy, xylem.

(B) Differences in YFP and YFP-TCTP1 appearance in wild-type roots of plants grafted with YFP- and YFP-TCTP1-expressing shoots. Red arrows indicate the presence of YFP, and white arrows indicate the absence of YFP signals.

(C) Distribution of YFP-TCTP1 in plants grafted with ethanol-inducible EtOH>>CoMV::mCherrySKL or EtOH>>CoMV::mCherrySKL/CALS3::sYFP root stocks. Upper panel shows longitudinal CLSM sections on EtOH>>CoMV::mCherrySKL and EtOH>>CoMV::mCherrySKL/CALS3::sYFP transgenic roots formed on plants grafted to 35S::YFP-TCTP1 shoots. Lower panel shows transverse CLSM sections on the same root tissue (dotted lines). Red arrows indicate the presence of both

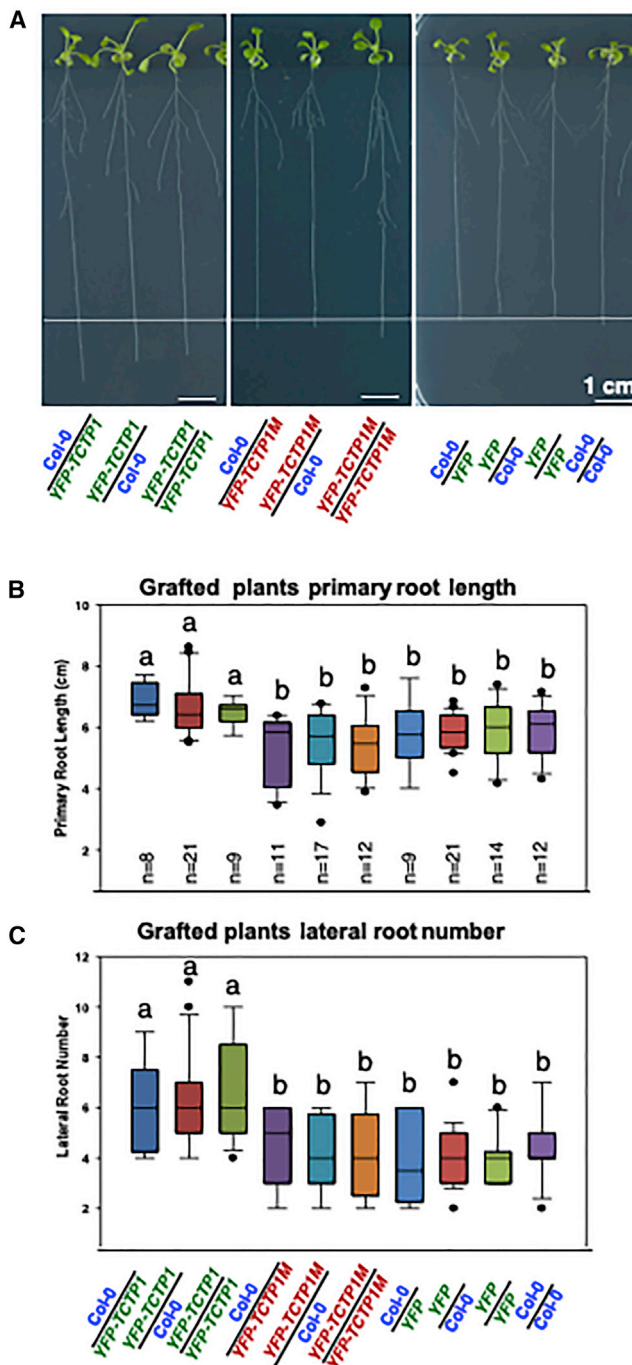


**Figure 5. Mobile *TCTP1* Transcript Promoting Root Formation**

(A) Representative images of analyzed grafted wild-type (Col-0) plants (14 days after grafting) expressing mobile *YFP-TCTP1* and non-mobile *YFP-TCTP1M* transcripts producing proteins with the same amino acid sequence. (B) Primary root length of grafted wild-type (Col-0) and transgenic plants. Note that wild-type plants producing mobile *YFP-TCTP1* transcript form significantly longer primary roots. Plants expressing the non-mobile *YFP-TCTP1M* transcript translated into a fusion protein with the same amino acid sequence as *YFP-TCTP1* show no changes in root length.

(C) Number of lateral root numbers formed on primary roots on grafted wild-type (Col-0) transgenic plants. As seen with primary root length, only grafted plants producing mobile *YFP-TCTP1* transcripts form significantly more lateral

for the detected growth changes, we analyzed the root growth in grafted plants expressing mobile *YFP-TCTP1* and non-mobile *YFP-TCTP1M* transcripts producing identical fusion proteins (Figure 5A; Figure S3G). We measured the primary root length (Figure 5B) and the number of lateral roots formed on primary roots (Figure 5C) of grafted wild-type (Col-0) and transgenic plants. With both measurements, we found that plants producing mobile *YFP-TCTP1* transcript form significantly longer primary and more lateral roots than non-transformed plants. In contrast, grafted plants expressing the non-mobile *YFP-TCTP1M* transcript translated into a fusion protein identical to *YFP-TCTP1* (Data S2G) showed no significant changes in root length or number of lateral roots compared with grafted wild type. This suggests that *TCTP1* mRNA mobility plays a crucial role in its function as growth regulator. Notably, although the *YFP-TCTP1* protein produced by *YFP-TCTP1M* is not transported to roots, it is not altered in its subcellular distribution (Figures S3 and S4). Thus, proper intercellular transfer guided by *TCTP1* mRNA seems to be a key factor for *TCTP1* function as a growth regulator in distant tissues.

## DISCUSSION

In this study, we identified  $m^5C$  mRNAs in *Arabidopsis* via MeRIP coupled with deep sequencing and with Nanopore RNA sequencing. Despite the different developmental stages and methods used, out of the 562  $m^5C$  RNAs identified in total, 96 were identified in at least 2, and 16 were identified in all 3 assays. Of the 562  $m^5C$  RNAs, >60% are assigned as mobile transcripts moving over graft junctions to distant tissues. Previous studies suggested that  $m^5C$  methylation increases the stability of tRNAs and potentially also of mRNAs in *Arabidopsis* [30, 31]. In line, we found that  $m^5C$  transcripts demonstrate a higher stability than expected by random chance (Figure S4B). However, our measurements on mRNA stability and abundance of  $m^5C$  mRNAs in *dmnt2 nsun2b* showed no significant changes. We did not detect an increase or decrease in abundance according to half-life and qRT-PCR assays with endogenous mobile *TCTP1*, *CAT3*, and *CK1* transcripts in methylation-deficient mutants, which suggests that  $m^5C$  does not change the stability of mobile transcripts (Figure 3D; Figure S4D).

The identified  $m^5C$  mRNA population is highly enriched in the mRNA population that is moving to distant tissues. Confirming that cytosine methylation plays a crucial role in mRNA transport, we found that lack of mRNA methylation activity in *dmnt2 nsun2b* mutants results in a lack of *YFP-TCTP1* and *HSC70.1* mobility. Furthermore, Aza treatment, which inhibits RNA methylation, resulted in a lack of *YFP-TCTP1* detection in roots of grafted plants whereas YFP protein diffusion from shoot to root remained intact (Figure 3). Both the lack of *YFP-TCTP1M* transcript mobility and the failure to detect the produced protein, which is identical to *YFP-TCTP1*, in grafted wild-type roots (Figure 2) suggest that

roots. In boxplots, boxes indicate variation between the datasets and means, n is the number of grafted plants analyzed, error bars represent  $\pm$ SE, and black dots represent measurements out of range  $\pm$  SE; significance was calculated with Student's t test (two tails), and the p value is indicated by a and b: ab < 0.05.

See also Figure S5.

full-length YFP-TCTP1 protein is not diffusing or actively transported from scions to roots. This seems to be contradicted by the finding that some proteins produced by *YFP-TCTP1* deletion variants lacking RNA mobility are still detected in roots (Figure 2; Figure S5D). For example, the small YFP-TCTP1Δ5′Δ3′ fusion protein is present in grafted wild-type roots but, as seen with YFP, its protein presence does not correlate with its transcript presence in roots (Figure 2; Figure S5D) suggesting that this truncated fusion is diffusing similarly to YFP via the phloem to roots.

Notably, compared with wild-type *TCTP1* RNA, the modified and non-mobile *YFP-TCTP1M* RNA sequence carries instead of the potential m<sup>5</sup>C-modified C<sub>141</sub> a T<sub>141</sub> ORF base (sequence CCAAUCCAUCU changed to CTAUCCAUCU; Data S2G). As this *YFP-TCTP1M* RNA fusion construct is not mobile over graft junctions (Figure 2D), it is likely that methylation of *TCTP1* bases mediates transcript transfer. Taking into account that transport of *HSC70.1* transcript also depends on m<sup>5</sup>C editing (Figure 3), these results suggest that mobile transcripts harbor an RNA motif recognized by RNA methyltransferases leading to cytosine methylation-mediated delivery of these transcripts into the phloem. After transport to roots and unloading e.g., into phloem pole pericycle cells (Figure 4), these mobile transcripts can be translated to functional proteins.

In *Arabidopsis*, *TCTP1* is ubiquitously and relatively highly expressed and a lack of *TCTP1* activity results in embryo abortion, lower number of secondary roots, and severely dwarfed plants with fewer cells [42, 43]. *TCTP1* protein, in line with a systemic function in other eukaryotes, has been detected in the *Arabidopsis* pollen tube secretome [44], and it was proposed that *TCTP1* protein has a function in root development [42, 45], suggesting that *TCTP1* RNA transport to specific lateral root initiation sites (Figure 4) might be part of its signaling function. The function of the relatively lowly expressed *Arabidopsis TCTP1* ortholog *TCTP2* was not examined in *Arabidopsis thaliana* but in transgenic *Nicotiana tabacum* plants. Here, *TCTP2* transcript moves long distance from source to sink tissues and less efficiently in the opposite direction. *TCTP2* protein and/or mRNA appeared in parenchyma cells and adventitious roots, correlating with adventitious root formation [46, 47]. In line, we have shown that transport of *TCTP1* transcript is a key to its function as a growth regulator. Proper *TCTP1* transcript folding is necessary for its transport to distant root cells as indicated by the lack of mobility of the *YFP-TCTP1M* transcript having an *Arabidopsis* optimized codon usage. *YFP-TCTP1M* transgenic plants express a fusion protein identical to YFP-TCTP1 protein with a similar subcellular distribution (Figure 2; Figure S3; Data S2). However, the *YFP-TCTP1M* produced protein does not induce root growth in plants (Figure 5) indicating that *TCTP1* transcript mobility is required for its growth regulating function.

Notably, measurements of mRNA stability and quantity revealed no changes of *TCTP1* or other tested mobile transcripts in cytosine methylation mutants (Figure 3; Figure S4D). Thus, mRNA abundance is most likely not a factor triggering transcript transport in contrast to proposed models based on *in silico* analyses [10, 11]. Our study suggests that cytosine methylation is present in a high number of mobile transcripts (>350) in

*Arabidopsis* (Figure 1C) and that a deficiency in mRNA methylation blocks transcript mobility. These combined results indicate that m<sup>5</sup>C methylation is at least one key factor eliciting mRNA long-distance transport over graft junctions.

In pumpkin, TCTP protein is present in phloem RNA BINDING PROTEIN 50 (RBP50)—protein complexes that bind to aforementioned PTB RNA sequences found in graft mobile *GAI* transcript [22, 48, 49]. Similarly, in potato RBP50 interacts with PTB-related sequences present in the 3′ UTR of graft mobile *StBEL5* transcript [50]. Consequently, PTB sequences were suggested to constitute bona fide motifs facilitating delivery of mRNAs into and/or out of the phloem stream [22]. However, neither a PTB-like motif nor a TLS motif is present in the *TCTP1* protein-coding sequences (ORFs). In the mobile *HSC70.1* transcript, several PTB-like motifs were detected, but a TLS motif was not found [1, 2]. Thus, one might conclude that both motifs are imperfect predictors for mRNA mobility. However, both PTB-like and TLS motifs are enriched in significant but small subsets of mobile transcripts. Thus, it seems that diverse mRNA transport initiator sequences exist to trigger mRNA transport. These transport mediating sequences could involve specific sequence stretches such as PTB-like sequences, structures like the TLS-related motif, or, as detected in a large fraction of mobile transcripts, an m<sup>5</sup>C methylation base modification, or combinations thereof, guiding the delivery and expression of mRNAs in specific cell types.

## STAR★METHODS

Detailed methods are provided in the online version of this paper and include the following:

- KEY RESOURCES TABLE
- LEAD CONTACT AND MATERIALS AVAILABILITY
- EXPERIMENTAL MODEL AND SUBJECT DETAILS
- METHOD DETAILS
  - EtOH-Inducible Expression Constructs
  - Methylated RNA Immuno-precipitation (MeRIP)
  - Sequencing and Analysis of MeRIP
  - Nanopore Sequencing and Analysis
  - Arabidopsis Hypocotyl Grafting
  - Expression Constructs
  - RNA and Protein Isolation
  - Reverse Transcription Reaction and PCR
  - Quantitative RT-PCR Assays
  - Western Blotting
  - 5-Azacytidine (Aza) Treatment
  - Microscopy
  - Analysis of mRNA Stability
- QUANTIFICATION AND STATISTICAL ANALYSIS
  - Data Processing and Statistical Analysis
  - Quantitative RT-PCR
  - Plant Growth Quantification
- DATA AND CODE AVAILABILITY

## SUPPLEMENTAL INFORMATION

Supplemental Information can be found online at <https://doi.org/10.1016/j.cub.2019.06.042>.



## ACKNOWLEDGMENTS

We thank Dana Schindelasch (MPI-MPP), Marina Stratmann (MPI-MPP), and Eike Kamann (University of Potsdam) for their excellent technical support and Frank Marchin (MPI-MPP) for comments on the manuscript. V.P. thanks Thomas Jenuwein for his support at MPI-IE Freiburg, where she established the MeRIP protocol used in the study. We thank Iain Robert Searle (University of Adelaide) for providing  $m^3C$  methylation-deficient mutant seeds and Marcin Janowski and Marek Mutwil (MPI-MPP) for the *UBQ10::HSC70.1-GFP* lines. This work was supported by Investissements d'Avenir ANR-10-LABX-54 MEMO LIFE and ANR-11-IDEX-0001-02 PSL\* Research University to V.C., DFG project A5, CRC 973 to B.M.-R., MPI-MPP internal funds to F.K., a Chinese Scholarship Council PhD stipend to L.Y., an EMBO Long-Term Fellowship to V.P., and an IMPRS PhD stipend to E.S. Part of the project was supported by ERC-Syg PLAMORF grant money awarded to F.K.

## AUTHOR CONTRIBUTIONS

V.P., S.Z., V.C., and F.K. conceived the idea of the project; L.Y., F.K., V.P., E. Saplaoura, N.P., and S.Z. performed experiments; L.Y. produced transgenic plants, performed all grafting and growth experiments, and with W.Z. produced *TCTP1* deletion constructs; E. Sokolowska produced the ethanol-inducible transgenic plants; F.A., E. Saplaoura, M.B., A.K., and A.G. analyzed the RNA-seq data; B.M.-R. and J.O. provided infrastructure and suggested experiments performed by J.O.; M.H. suggested experiments and supervised experiments performed by N.P.; F.K. with L.Y., E. Saplaoura, V.P., and F.A. wrote the manuscript with input from V.C., M.H., and B.M.-R. All authors read the manuscript and expressed their consent to submit the final version of the manuscript.

## DECLARATION OF INTERESTS

The authors declare no competing interests.

Received: January 31, 2019

Revised: May 8, 2019

Accepted: June 13, 2019

Published: July 18, 2019

## REFERENCES

- Thieme, C.J., Rojas-Triana, M., Stecyk, E., Schudoma, C., Zhang, W., Yang, L., Miñambres, M., Walther, D., Schulze, W.X., Paz-Ares, J., et al. (2015). Endogenous Arabidopsis messenger RNAs transported to distant tissues. *Nat. Plants* 1, 15025.
- Zhang, Z., Zheng, Y., Ham, B.K., Chen, J., Yoshida, A., Kochian, L.V., Fei, Z., and Lucas, W.J. (2016). Vascular-mediated signalling involved in early phosphate stress response in plants. *Nat. Plants* 2, 16033.
- Xia, C., Zheng, Y., Huang, J., Zhou, X., Li, R., Zha, M., Wang, S., Huang, Z., Lan, H., Turgeon, R., et al. (2018). Elucidation of the mechanisms of long-distance mRNA movement in a *Nicotiana benthamiana*/Tomato hetero-graft system. *Plant Physiol.* 177, 745–758.
- Yang, Y., Mao, L., Jittayasothorn, Y., Kang, Y., Jiao, C., Fei, Z., and Zhong, G.Y. (2015). Messenger RNA exchange between scions and rootstocks in grafted grapevines. *BMC Plant Biol.* 15, 251.
- Nevo-Dinur, K., Govindarajan, S., and Amster-Choder, O. (2012). Subcellular localization of RNA and proteins in prokaryotes. *Trends Genet.* 28, 314–322.
- Medioni, C., Mowry, K., and Besse, F. (2012). Principles and roles of mRNA localization in animal development. *Development* 139, 3263–3276.
- Weis, B.L., Schleiff, E., and Zerges, W. (2013). Protein targeting to subcellular organelles via mRNA localization. *Biochim. Biophys. Acta* 1833, 260–273.
- Tian, L., Chou, H.L., Zhang, L., Hwang, S.K., Starkenburg, S.R., Doroshenko, K.A., Kumamaru, T., and Okita, T.W. (2018). RNA-Binding Protein RBP-P is required for glutelin and prolamine mRNA localization in rice endosperm cells. *Plant Cell* 30, 2529–2552.
- Kehr, J., and Kragler, F. (2018). Long distance RNA movement. *New Phytol.* 218, 29–40.
- Calderwood, A., Kopriva, S., and Morris, R.J. (2016). Transcript abundance explains mRNA mobility data in *Arabidopsis thaliana*. *Plant Cell* 28, 610–615.
- Morris, R.J. (2018). On the selectivity, specificity and signalling potential of the long-distance movement of messenger RNA. *Curr. Opin. Plant Biol.* 43, 1–7.
- Lucas, W.J., Bouché-Pillon, S., Jackson, D.P., Nguyen, L., Baker, L., Ding, B., and Hake, S. (1995). Selective trafficking of KNOTTED1 homeodomain protein and its mRNA through plasmodesmata. *Science* 270, 1980–1983.
- Kragler, F., Lucas, W.J., and Monzer, J. (1998). Plasmodesmata: Dynamics, domains and patterning. *Ann. Bot. (Lond.)* 81, 1–10.
- Kragler, F., Monzer, J., Shash, K., Xoconostle-Cázares, B., and Lucas, W.J. (1998). Cell-to-cell transport of proteins: requirement for unfolding and characterization of binding to a putative plasmodesmal receptor. *Plant J.* 15, 367–381.
- Ross-Elliott, T.J., Jensen, K.H., Haaning, K.S., Wager, B.M., Knoblauch, J., Howell, A.H., Mullendore, D.L., Monteith, A.G., Paultre, D., Yan, D., et al. (2017). Phloem unloading in Arabidopsis roots is convective and regulated by the phloem-pole pericycle. *eLife* 6, e24125.
- Zhang, W., Thieme, C.J., Kollwig, G., Apelt, F., Yang, L., Winter, N., Andresen, N., Walther, D., and Kragler, F. (2016). tRNA-related sequences trigger systemic mRNA transport in plants. *Plant Cell* 28, 1237–1249.
- Paultre, D.S.G., Gustin, M.P., Molnar, A., and Oparka, K.J. (2016). Lost in transit: Long-distance trafficking and phloem unloading of protein signals in Arabidopsis homografts. *Plant Cell* 28, 2016–2025.
- Huang, N.C., and Yu, T.S. (2009). The sequences of Arabidopsis *GA-INSENSITIVE RNA* constitute the motifs that are necessary and sufficient for RNA long-distance trafficking. *Plant J.* 59, 921–929.
- Li, C., Zhang, K., Zeng, X., Jackson, S., Zhou, Y., and Hong, Y. (2009). A cis element within *flowering locus T* mRNA determines its mobility and facilitates trafficking of heterologous viral RNA. *J. Virol.* 83, 3540–3548.
- Haywood, V., Yu, T.S., Huang, N.C., and Lucas, W.J. (2005). Phloem long-distance trafficking of *GIBBERELLIC ACID-INSENSITIVE RNA* regulates leaf development. *Plant J.* 42, 49–68.
- Cho, S.K., Sharma, P., Butler, N.M., Kang, I.H., Shah, S., Rao, A.G., and Hannapel, D.J. (2015). Polypyrimidine tract-binding proteins of potato mediate tuberization through an interaction with *StBEL5* RNA. *J. Exp. Bot.* 66, 6835–6847.
- Ham, B.K., Brandom, J.L., Xoconostle-Cázares, B., Ringgold, V., Lough, T.J., and Lucas, W.J. (2009). A polypyrimidine tract binding protein, pumpkin RBP50, forms the basis of a phloem-mobile ribonucleoprotein complex. *Plant Cell* 21, 197–215.
- Zhang, S., Sun, L., and Kragler, F. (2009). The phloem-delivered RNA pool contains small noncoding RNAs and interferes with translation. *Plant Physiol.* 150, 378–387.
- Burgess, A.L., David, R., and Searle, I.R. (2015). Conservation of tRNA and rRNA 5-methylcytosine in the kingdom Plantae. *BMC Plant Biol.* 15, 199.
- Zhang, X., Liu, Z., Yi, J., Tang, H., Xing, J., Yu, M., Tong, T., Shang, Y., Gorospe, M., and Wang, W. (2012). The tRNA methyltransferase NSun2 stabilizes p16INK4 mRNA by methylating the 3'-untranslated region of p16. *Nat. Commun.* 3, 712.
- Karjilovich, J., Kantartzis, A., and Yu, Y.-T. (2010). RNA modifications: a mechanism that modulates gene expression. *Methods Mol. Biol.* 629, 1–19.
- Roundtree, I.A., Evans, M.E., Pan, T., and He, C. (2017). Dynamic RNA modifications in gene expression regulation. *Cell* 169, 1187–1200.
- Sibbritt, T., Patel, H.R., and Preiss, T. (2013). Mapping and significance of the mRNA methylome. *Wiley Interdiscip. Rev. RNA* 4, 397–422.

29. Meyer, K.D., Saletore, Y., Zumbo, P., Elemento, O., Mason, C.E., and Jaffrey, S.R. (2012). Comprehensive analysis of mRNA methylation reveals enrichment in 3' UTRs and near stop codons. *Cell* **149**, 1635–1646.
30. David, R., Burgess, A., Parker, B., Li, J., Pulsford, K., Sibbritt, T., Preiss, T., and Searle, I.R. (2017). Transcriptome-Wide Mapping of RNA 5-Methylcytosine in *Arabidopsis* mRNAs and Noncoding RNAs. *Plant Cell* **29**, 445–460.
31. Cui, X., Liang, Z., Shen, L., Zhang, Q., Bao, S., Geng, Y., Zhang, B., Leo, V., Vardy, L.A., Lu, T., et al. (2017). 5-Methylcytosine RNA methylation in *Arabidopsis thaliana*. *Mol. Plant* **10**, 1387–1399.
32. Macke, T.J., Ecker, D.J., Gutell, R.R., Gautheret, D., Case, D.A., and Sampath, R. (2001). RNAMotif, an RNA secondary structure definition and search algorithm. *Nucleic Acids Res.* **29**, 4724–4735.
33. Bailey, T.L. (2011). DREME: motif discovery in transcription factor ChIP-seq data. *Bioinformatics* **27**, 1653–1659.
34. Narsai, R., Howell, K.A., Millar, A.H., O'Toole, N., Small, I., and Whelan, J. (2007). Genome-wide analysis of mRNA decay rates and their determinants in *Arabidopsis thaliana*. *Plant Cell* **19**, 3418–3436.
35. Zuker, M., and Stiegler, P. (1981). Optimal computer folding of large RNA sequences using thermodynamics and auxiliary information. *Nucleic Acids Res.* **9**, 133–148.
36. Lorenz, R., Bernhart, S.H., Höner Zu Siederdissen, C., Tafer, H., Flamm, C., Stadler, P.F., and Hofacker, I.L. (2011). ViennaRNA Package 2.0. *Algorithms Mol. Biol.* **6**, 26.
37. Proctor, J.R., and Meyer, I.M. (2013). COFOLD: an RNA secondary structure prediction method that takes co-transcriptional folding into account. *Nucleic Acids Res.* **41**, e102.
38. Warren, L., Manos, P.D., Ahfeldt, T., Loh, Y.H., Li, H., Lau, F., Ebina, W., Mandal, P.K., Smith, Z.D., Meissner, A., et al. (2010). Highly efficient reprogramming to pluripotency and directed differentiation of human cells with synthetic modified mRNA. *Cell Stem Cell* **7**, 618–630.
39. Lin, M.K., Lee, Y.J., Lough, T.J., Phinney, B.S., and Lucas, W.J. (2009). Analysis of the pumpkin phloem proteome provides insights into angiosperm sieve tube function. *Mol. Cell. Proteomics* **8**, 343–356.
40. Giavalisco, P., Kapitza, K., Kolasa, A., Buhtz, A., and Kehr, J. (2006). Towards the proteome of *Brassica napus* phloem sap. *Proteomics* **6**, 896–909.
41. Vatén, A., Dettmer, J., Wu, S., Stierhof, Y.D., Miyashima, S., Yadav, S.R., Roberts, C.J., Campilho, A., Bulone, V., Lichtenberger, R., et al. (2011). Callose biosynthesis regulates symplastic trafficking during root development. *Dev. Cell* **21**, 1144–1155.
42. Berkowitz, O., Jost, R., Pollmann, S., and Masle, J. (2008). Characterization of TCTP, the translationally controlled tumor protein, from *Arabidopsis thaliana*. *Plant Cell* **20**, 3430–3447.
43. Betsch, L., Savarin, J., Bendahmane, M., and Szecsi, J. (2017). Roles of the translationally controlled tumor protein (TCTP) in plant development. *Results Probl. Cell Differ.* **64**, 149–172.
44. Hafidh, S., Potěšil, D., Fila, J., Čapkova, V., Zdráhal, Z., and Honys, D. (2016). Quantitative proteomics of the tobacco pollen tube secretome identifies novel pollen tube guidance proteins important for fertilization. *Genome Biol.* **17**, 81.
45. Branco, R., and Masle, J. (2019). Systemic signalling through translationally controlled tumour protein controls lateral root formation in *Arabidopsis*. *J. Exp. Bot.* Published online April 30, 2019. <https://doi.org/10.1093/jxb/erz204>.
46. Toscano-Morales, R., Xoconostle-Cázares, B., Cabrera-Ponce, J.L., Hinojosa-Moya, J., Ruiz-Salas, J.L., Galván-Gordillo, S.V., Guevara-González, R.G., and Ruiz-Medrano, R. (2015). AtTCTP2, an *Arabidopsis thaliana* homolog of Translationally Controlled Tumor Protein, enhances *in vitro* plant regeneration. *Front. Plant Sci.* **6**, 468.
47. Toscano-Morales, R., Xoconostle-Cázares, B., Martínez-Navarro, A.C., and Ruiz-Medrano, R. (2016). AtTCTP2 mRNA and protein movement correlates with formation of adventitious roots in tobacco. *Plant Signal. Behav.* **11**, e1071003.
48. Li, P., Ham, B.K., and Lucas, W.J. (2011). CmRBP50 protein phosphorylation is essential for assembly of a stable phloem-mobile high-affinity ribonucleoprotein complex. *J. Biol. Chem.* **286**, 23142–23149.
49. Ham, B.K., and Lucas, W.J. (2017). Phloem-mobile RNAs as systemic signaling agents. *Annu. Rev. Plant Biol.* **68**, 173–195.
50. Hannapel, D.J., Sharma, P., Lin, T., and Banerjee, A.K. (2017). The Multiple Signals That Control Tuber Formation. *Plant Physiol.* **174**, 845–856.
51. Schindelin, J., Arganda-Carreras, I., Frise, E., Kaynig, V., Longair, M., Pietzsch, T., Preibisch, S., Rueden, C., Saalfeld, S., Schmid, B., et al. (2012). Fiji: an open-source platform for biological-image analysis. *Nat. Methods* **9**, 676–682.
52. Dobin, A., Davis, C.A., Schlesinger, F., Drenkow, J., Zaleski, C., Jha, S., Batut, P., Chaisson, M., and Gingeras, T.R. (2013). STAR: ultrafast universal RNA-seq aligner. *Bioinformatics* **29**, 15–21.
53. Zhang, Y., Liu, T., Meyer, C.A., Eickhout, J., Johnson, D.S., Bernstein, B.E., Nusbaum, C., Myers, R.M., Brown, M., Li, W., and Liu, X.S. (2008). Model-based analysis of ChIP-Seq (MACS). *Genome Biol.* **9**, R137.
54. Deveau, Y., Peaucelle, A., Roberts, G.R., Coen, E., Simon, R., Mizukami, Y., Traas, J., Murray, J.A., Doonan, J.H., and Laufs, P. (2003). The ethanol switch: a tool for tissue-specific gene induction during plant development. *Plant J.* **36**, 918–930.
55. Martin, M. (2011). Cutadapt removes adapter sequences from high-throughput sequencing reads. *EMBnet J.* **17**, 10–12.
56. Earley, K.W., Haag, J.R., Pontes, O., Opper, K., Juehne, T., Song, K., and Pikaard, C.S. (2006). Gateway-compatible vectors for plant functional genomics and proteomics. *Plant J.* **45**, 616–629.
57. Wang, M., Zhao, Y., and Zhang, B. (2015). Efficient Test and Visualization of Multi-Set Intersections. *Sci. Rep.* **5**, 16923.
58. Apelt, F., Breuer, D., Nikoloski, Z., Stitt, M., and Kragler, F. (2015). Phytotyping(4D): a light-field imaging system for non-invasive and accurate monitoring of spatio-temporal plant growth. *Plant J.* **82**, 693–706.

## STAR★METHODS

## KEY RESOURCES TABLE

REAGENT or RESOURCE	SOURCE	IDENTIFIER
<b>Antibodies</b>		
Rat monoclonal [3H9] to GFP	ChromoTek	Cat#: 029762
Anti-Rat IgG—Peroxidase	Sigma-Aldrich	Cat#: A9037
Anti-5-methylcytosine	ZymoResearch	Cat#: A3001-200
<b>Bacterial Strains</b>		
TOP 10 <i>E. coli</i> strain	Thermo Fisher	Cat#: C404010
DB3.1 <i>E. coli</i> strain	Invitrogen	Cat#: 11782-018
AGL1 <i>Agrobacteria</i> strain for transformation	Lab inoculate	N/A
<b>Chemicals, Peptides, and Recombinant Proteins</b>		
TRIzol Reagent	Invitrogen	Cat#: 15596026
Micro agar	Duchefa Biochemie	Cat#: 9002-18-0
DreamTaq DNA Polymerase	Thermo Scientific	Cat#: EP0712
ECL Prime Western Blotting Detection Reagent	GE Healthcare	Cat#: RPN2232
5-Azacytidine	Sigma-Aldrich	Cat#: 320-67-2
Actinomycin D	Sigma-Aldrich	Cat#: 50-76-0
<b>Critical Commercial Assays</b>		
TURBO-DNAfree kit	Invitrogen	Cat#: AM1907
Oligotex mRNA mini kit	QIAGEN	Cat#: 70022
RiboMinus Plant kit	Invitrogen	Cat#: A1083808
<i>TCTP1M</i> gene synthesis	IDT Genomics	N/A
Direct RNA sequencing kit RNA001	Nanopore company	SQK-RNA001
SuperScript III Reverse Transcriptase	Thermo Fischer	Cat#: 18080044
mRNA purification kit	Invitrogen	Cat#: 61006
T4 DNA ligase	NEB	Cat#: M0202M
Bioanalyzer RNA 6000 Nano kit	Agilent	Cat#: 5067-1511
<b>Deposited Data</b>		
The datasets generated and analyzed during the current study	NCBI Sequencing Read Archive (SRA) BioProject ID: PRJNA498623	N/A
<b>Experimental Models: Organisms/Strains</b>		
<i>Arabidopsis thaliana</i> Col-0 wild type	MPIMP, sequenced by FK lab	N/A
<i>Arabidopsis thaliana</i> Col0 <i>hsc70.1</i> mutant	<i>Arabidopsis</i> resource stock center	TAIR# AT5G02500, SALK_135531.41.60
<i>Arabidopsis thaliana</i> Col0 <i>dnmt2 nsun2b</i> mutant	[24]	N/A
<b>Oligonucleotides</b>		
pENTR4 vector	Thermo Fisher	Cat#: A10465
pEarleyGate 104	<i>Arabidopsis</i> resource stock center	N/A
Oligonucleotides, PCR primers	Data S2	N/A
<b>Recombinant DNA</b>		
35S::YFP- <i>TCTP1</i> fusion/deletion constructs	See STAR Methods and Data S2	N/A
CoYMV::alcR >> alcA::mCherrySKL >> CalS3::YFP	See STAR Methods	N/A
UBQ10::HSC70.1-GFP	See STAR Methods	N/A
<b>Software and Algorithms</b>		
Fiji, ImageJ package, Version 2.0.0-rc-69	[51]	<a href="https://fiji.sc/#">https://fiji.sc/#</a>
TOMBO		<a href="https://github.com/nanoporetech/tombo">https://github.com/nanoporetech/tombo</a>
FastQC		<a href="https://www.bioinformatics.babraham.ac.uk/projects/fastqc">https://www.bioinformatics.babraham.ac.uk/projects/fastqc</a>
STAR	[52]	N/A
MACS2	[53]	N/A



## LEAD CONTACT AND MATERIALS AVAILABILITY

Further information and requests for resources and reagents should be directed to and will be fulfilled by the Lead Contact, Friedrich Kragler ([kragler@mpimp-golm.mpg.de](mailto:kragler@mpimp-golm.mpg.de)).

This study did not generate new unique reagents. Plasmids and transgenic *Arabidopsis thaliana* lines generated in this study are available upon request without restrictions.

## EXPERIMENTAL MODEL AND SUBJECT DETAILS

*Arabidopsis thaliana* ecotype Columbia-0 (Col-0) wild-type, transgenic, and mutant seeds were sterilized by 70% ethanol supplemented with 1% Tween20 for 5 minutes (note: for EtOH-inducible *mCherrySKL* and *CalS3:sYFP* lines this step was avoided), 3% sodium hypochlorite for 5 minutes, washed 5 times with sterile distilled water, and resuspended with 0.15% agar. Seedlings were grown on plates, in Percival growth chambers set to either long days (16 h light / 8 h dark, 22°C, light intensity:  $170 \mu\text{E} \cdot \text{m}^{-2} \cdot \text{s}^{-1}$ ) or short days (8 h light / 16 h dark, 22°C, light intensity:  $170 \mu\text{E} \cdot \text{m}^{-2} \cdot \text{s}^{-1}$ ). For the MeRIP assays of seedlings, *Arabidopsis* wild-type (Col-0) were grown in half-strength (1/2) Murashige and Skoog (MS) liquid medium supplemented with 0.5 g/l MES buffer and 7 g/l sucrose (0.7%), adjusted to pH 5.8 with KOH. Twenty-five ml of medium was used per each 100 mm x 100 mm x 20 mm Petri dish containing 50 - 80 seeds. The cultures were grown in Percival growth chambers with 12 h light / 12 h dark (day 22°C / night 19°C; light intensity:  $170 \mu\text{E} \cdot \text{m}^{-2} \cdot \text{s}^{-1}$ ) and harvested for RNA extraction 10 days after germination. For the m<sup>5</sup>C transcriptome analysis of adult plants, *A. thaliana* Col-0 were grown on soil in growth chambers under long day conditions 16 h light / 8 h dark; day 22°C / night 19°C; light intensity:  $79 \mu\text{E} \cdot \text{m}^{-2} \cdot \text{s}^{-1}$ ; 6 Klux; 60% relative humidity. The light was produced by Neon tubes T5 (ref: OSRAM Lumilux DE LUX cool Daylight HO49W/965). For transformation and propagation, adult plants were grown on soil in growth chambers under long-day condition (16 h light / 8 h dark; day 22°C / night 19°C; light intensity:  $170 \mu\text{E} \cdot \text{m}^{-2} \cdot \text{s}^{-1}$ ; relative humidity: 60%) or under short-day condition (8 h light / 16 h dark; day 22°C / night 19°C; light intensity:  $170 \mu\text{E} \cdot \text{m}^{-2} \cdot \text{s}^{-1}$ ; relative humidity: 60%). *hsc70.1* insertion mutant (TAIR# AT5G02500, SALK\_135531.41.60) seeds were obtained from the *Arabidopsis* resource stock center (ABRC). *dnmt2* (SALK\_136635) *nsun2b* (SAIL\_667\_D03) double knock-out mutant seeds were kindly provided by [24].

## METHOD DETAILS

### EtOH-Inducible Expression Constructs

Full-length *CALS3* CDS sequence (TAIR# AT5G13000) was PCR-amplified from an *A. thaliana* Col-0 cDNA library and cloned into pENTRY4 vector MCS (Invitrogen) using *NcoI* and *XbaI*. *YFP* was fused in frame into *CALS3* ORF between base +1462 and +1463 by PCR using *EcoRI* and *XhoI* restriction sites and 5 x Ala (GCT) linker sequences (Table S1). The resulting ENTRY clone was recombined (gateway reaction) into the alcohol inducible binary destination vector pEC2 (HygR) [54]. The *pEC2-CALS3:sYFP* binary expression vector was introduced into the *Agrobacterium* strain GV3101 to transform Col-0 wild-type. Resulting transgenic lines were confirmed by genomic PCR and crossed with transgenic lines containing the binary vector pSRN (KanR) harboring the companion cell-specific and ethanol-inducible *CoYMV::alcR alcA::mCherrySKL* constructs (Figures S5A and S5B; Table S1). EtOH induction was performed 7 days after grafting on plants grown on plates (0.5 MS, 1% sucrose) by evaporation of 10% EtOH in a closed container in a Percival growth chamber for 24 h under long-day conditions as described above.

### Methylated RNA Immuno-precipitation (MeRIP)

Total RNA was purified from 10-day-old seedlings or leaves from 6-week-old adult plants. RNA isolation was performed using TRIzol (Ambion) according to the manufacturer's instructions. Instead of chloroform, 1-bromo,3-chloro-propane was used to improve DNA/RNA separation. Quality controlled (Bioanalyzer RNA 6000 Nano Kit; Agilent) RNA samples were DNase I digested following the protocol supplied by TURBO-DNAfree Kit (Ambion) and, for the seedling samples, also ribo-depleted using the RiboMinus Plant Kit for RNA-Seq (Invitrogen). The treated RNA samples were sonicated (Covaris S220 sonication system; microtube AFA Fiber Pre-Slit Snap-Cap 6 x 16 mm [Lot No 002516, Part No 520045]), to yield an average size of 100 nt (confirmed by Bioanalyzer RNA 6000 Nano Kit; Agilent) and then used as input material for RNA immunoprecipitation (RIP) with an antibody specifically binding to m<sup>5</sup>C nucleotides present in single-stranded nucleic acids (AB Clone 10G4, Zymo Research). For this purpose 12.5  $\mu\text{g}$  of sonicated RNA and H<sub>2</sub>O up to 100  $\mu\text{L}$  were added in low binding tubes, incubated for 10 min at 70°C in a water bath and cooled down 10 minutes on ice-water mix. 20  $\mu\text{L}$  of the RNA were saved as the Input sample (freeze at -80°C). The residual 80  $\mu\text{L}$  were filled with H<sub>2</sub>O up to 1720  $\mu\text{L}$  and distribute the solution to 4 low-binding tubes: 430  $\mu\text{L}$  for each of the 3 IPs and 430  $\mu\text{L}$  for the mock sample (without antibody). Each reaction was supplied with 50  $\mu\text{L}$  10x MeRIP buffer (100 mM Na-Phosphate pH 7.0, 1.4 M NaCl, 0.5% Triton X-100), 10  $\mu\text{L}$   $\alpha$ -5mC antibody (1  $\mu\text{g}/\mu\text{L}$ , ZymoResearch) in the IP samples or 10  $\mu\text{L}$  of H<sub>2</sub>O in the Mock sample and 10  $\mu\text{L}$  RNasin Plus 40 U/ $\mu\text{L}$  (Promega). The tubes were incubated 12 - 14 hours at 4°C rotating overhead. The protein G magnetic beads were prepared immediately before addition by washing three times for 5 minutes with 1x MeRIP buffer (800  $\mu\text{L}$  buffer for 40  $\mu\text{L}$  beads). The beads were resuspended in the same volume of 1x MeRIP buffer as taken initially and 40  $\mu\text{L}$  of prepared beads were added to each sample. The samples kept rotating overhead for 2 more hours at 4°C. After the end of incubation time the samples were placed on the magnetic rack and the liquid was removed (discarded or saved for controls). Five washing steps followed by resuspending the beads in

700  $\mu$ L of 1x MeRIP buffer supplied with 0.01% Tween 20 and incubating for 10 min at RT, rotating overhead. After the last wash, the beads were resuspended in 200  $\mu$ L Proteinase K digestion buffer (50 mM Tris-HCl, pH 8.0, 10mM EDTA, 0.5% SDS) with 3.5  $\mu$ L RNase grade Proteinase K from Ambion (20mg/mL stock RNase free) and incubated at 50°C for 3 hours on a shaker.

The extraction of RNA was then performed by adding 800  $\mu$ L Trizol (Ambion) per sample and according to the manufacturer's protocol. Glycoblue was added to precipitate RNA and all tubes were pre-cooled to be used in the precipitation step. All RNA samples were resuspended in 20  $\mu$ L RNase-free H<sub>2</sub>O. To use in qPCR assays, reverse transcription was done following the AMV Reverse Transcriptase protocol (Promega) with random hexamers. TruSeq RNA v2 was chosen as the RNA-seq library prep kit (directional) for deep sequencing of the INPUT and IP samples from *Arabidopsis* seedlings (for sample replicates and sequencing details see Table S2). IP RNA samples from *Arabidopsis* rosette leaves were deep sequenced with Hiseq4000 SE50 and the Input RNA with BGISEQ-500 SE50.

The such enriched and fragmented MeRIP RNA was used for RNA-seq. Seedling *A. thaliana* Col-0 m<sup>5</sup>C RNA samples (input RNA used as reference) and three parallel MeRIPs (technical replicates) performed on 2.5  $\mu$ g RNA (each ribo-depleted and sonicated RNA) and on one mock sample (negative control, beads with no antibody) were submitted to RNaseq. Ribominus plant Kit from Invitrogen (Catalog number: A1083808) was used to remove rRNA from the RNA samples. From 40  $\mu$ g of total RNA, about 12.5  $\mu$ g of ribo-depleted RNA were obtained in 80  $\mu$ L total volume. 4 different ribodepletion reactions were done at the same time, each with 10  $\mu$ g of RNA, for each of the two sets of plant cultures used in this study (a total of 8 ribodepletion reactions). This whole procedure was performed with two independent sets of seedling cultures (biological replicates), growing in parallel (manually randomized position) in the environmentally controlled chamber. For adult plants, 2.5  $\mu$ g of sonicated RNA were used for the input sample, the MeRIP assay, and the mock.

### Sequencing and Analysis of MeRIP

All MeRIP samples - two input and one IP sample for MeRIP seedlings; one input and one IP sample for MeRIP rosette leaves - were submitted to single-end sequencing with a read length of 50 bases (BGI, China) (Table S2). Reads were subjected to quality control with FastQC (<https://www.bioinformatics.babraham.ac.uk/projects/fastqc/>), non-anchored adaptors were trimmed from the 3' end of reads using cutadapt [55], and trimmed reads shorter than 48 nt were discarded. For seedling datasets, consistency between replicates was evaluated using Pearson's correlation ( $r = 0.91$ ). All trimmed reads were mapped to the *Arabidopsis* genome sequence (TAIR10 annotation) using STAR [52] allowing up to 6% of mismatches and intron sizes less than 10 kb. Uniquely mapping reads were retained for further analysis (note that we also discarded reads mapping around rDNA annotated regions on chromosome 2 and 3, as these regions are not well annotated). Reads failing the vendor/platform quality check (SAM flag 0x200) were discarded. In order to identify RNAs that potentially harbor m<sup>5</sup>C methylation sites, we used two different methods and only kept those reported by both methods. First, we adapted a previously published method for MeRIP-Seq peak detection [29]. We divided the entire *Arabidopsis* genome into 25-nt discrete, non-overlapping windows and counted, for Input and MeRIP (IP) samples, the number of uniquely mapped reads, considering only the last mapped nucleotide, within each window. The Fisher Exact Test (FET) was used to determine windows significantly enriched in each MeRIP sample (considered independently) compared to input. The Benjamini-Hochberg procedure was used to correct for multiple testing. Finally, independent q-values were combined using Fisher's method for each window and final q-values < 0.05 were considered significant. This strategy allowed us to identify MeRIP peaks with high confidence. Given that sequenced reads (48–50 nt) derive from 100-nt RNA fragments, we expect peaks to cover at least two consecutive windows. Thus, enriched windows that are singletons were discarded. Second, MeRIP peaks were also detected using MACS2 [53]; a peak caller typically used for ChIP-seq analysis. For downstream analysis, only transcripts found enriched by both methods were selected. Thus, for the MeRIP samples, we obtained two sets of m<sup>5</sup>C methylated transcripts identified by Meyer et al. and MACS2 peak calling for (i) seedlings identified independently in two replicates ( $n = 182$ ) and (ii) rosette leaves from adult plants identified in one replicate ( $n = 416$ ) (Data S1). Both lists overlap by 66 transcripts. MeRIP peak distribution along putative methylated transcripts was plotted using an *ad hoc* script that computes the surface covered by each detected MeRIP peak along a meta-transcript formed by the merged exons. Transcripts were sorted by length from top to bottom and were centered at the CDS start position. Additionally, we plotted the relative frequency of methylation sites across the relative lengths of the UTR and CDS regions.

### Nanopore Sequencing and Analysis

The nanopore sequenced samples are from 3-week-old soil grown seedlings. After total RNA extraction with TRIzol followed by DNase I treatment, mRNAs were enriched with oligotex mRNA mini kit (QIAGEN, Cat#: 70022). Around 500 ng mRNA were used for direct RNA sequencing library preparation. The library was constructed strictly with the protocol provided by the Nanopore company ([https://store.nanoporetech.com/media/wysiwyg/Example\\_Direct\\_RNA\\_Sequencing\\_Protocol\\_v4.pdf](https://store.nanoporetech.com/media/wysiwyg/Example_Direct_RNA_Sequencing_Protocol_v4.pdf)). The kit for the library preparation is SQK-RNA001. The prepared library was then loaded to R9.4 flowcell and sequenced with MinION device for 24 hours. The acquired fast5 files were analyzed with Tombo package (V 1.4) (<https://github.com/nanoporetech/tombo>) to predict the modifications of the RNA sequences. The model of "m5C" was implemented to detect possible cytosine modification in each read. The score on each site indicated the fraction of a possible modification on a given site and only the sites with > 90% fraction were selected for further analysis (Data S1).

### Arabidopsis Hypocotyl Grafting

*Arabidopsis* seeds were grown vertically on the plates (1/2 MS salts, 1% sucrose, and 0.68% micro agar [Duchefa Biochemie]) under short-day condition in a controlled environmental chamber (Percival) for 7–8 days. Seedlings with similar size and evenly elongated hypocotyls were cut in the upper half of the hypocotyl with a sterile razor blade. Silicon micro-tubing (0.3 mm internal diameter) was used to support graft junctions. Grafted plants were transferred to new plates (1/2 MS salts, 1% sucrose, 1% micro agar [Duchefa Biochemie]) and grown vertically under short-day condition. Adventitious roots forming above the junction were removed every two days. Ten days after grafting, plants were used to detect YFP fluorescence in the scion and stock using CLSM. Two weeks after grafting, scion and root tissues were harvested for RNA isolation and detection of transcripts by RT-PCR using oligo(dT) primer for the RT reaction and specific primers for the PCR amplification.

### Expression Constructs

To produce YFP reporter fusion with wild-type *TCTP1* and synthetic *TCTP1* (*TCTP1M*), the full-length wild-type CDS was PCR-amplified from a cDNA library (FK734/FK735) and *TCTP1M* was synthesized (IDT Genomics), respectively. Both of them were cloned into the pENTR4 (Addgene/Invitrogen) vector using *NcoI* and *XhoI* restriction sites and transferred into the pEarlygate104 binary vector [56] by LR recombinase reaction. For the *TCTP1Δ3'* (FK734/FK1201), *TCTP1Δ5'* (FK1202/FK735), and *TCTP1Δ5'Δ3'* (FK1203/FK1204) constructs, we used the same strategy. For the *TCTP1ΔA* (FK1205/FK1206) construct, two DNA fragments of *TCTP1ΔA* cDNAs were amplified by in-fusion PCR from the pENTR4-*TCTP1* template (Table S1), ligated into pENTR4-*TCTP1ΔA* (In-Fusion HD cloning Kit), and transferred into the pEarlygate104 binary vector by LR recombinase reaction (Data S2). All YFP-*TCTP1* constructs were verified by Sanger sequencing prior to introduction into the *Agrobacterium* strains GV3101 or ALG1, and transformation of Col-0 plants by double floral dipping.

### RNA and Protein Isolation

Grafted scion and stock tissues (from > 5 plants) were independently collected in 2 mL tubes containing metal beads. After freezing, 750  $\mu$ L TRIzol Reagent (Invitrogen) was added and samples were homogenized (20 s, vortex) and incubated for 5 minutes at room temperature (RT) to permit complete dissociation of the nucleoprotein complexes. After chloroform extraction (0.2 mL per 0.75 mL of TRIzol Reagent) the upper aqueous phase containing RNA was used for RNA isolation and the phenol phase for protein isolation (see below). The RNA phase was transferred to 1.5 mL RNase-free tubes and 1 volume isopropanol and 1/10 volume 3 M NaOAc (pH 5.2) were added to precipitate total RNA. The RNA pellets were washed twice with 1 mL ice-cold 80% ethanol and once with 1 mL 99% ethanol, resuspended in 10–25  $\mu$ L DEPC treated H<sub>2</sub>O, and stored at –80°C until further use. Protein isolation: the lower phenol phase (protein fraction) was submitted to protein precipitation by adding 1.5 mL isopropanol, incubate at RT for 10 min and centrifuge at 12000 g for 10 min at 4°C. The pellet was washed twice with 2 mL 0.3 M guanidine hydrochloride (in 95% ethanol) and incubation for 20 min at room temperature. After centrifugation (5 min, 7500 g at 4°C) the protein pellets were washed once with 99% ethanol and resuspended in 50 to 200  $\mu$ L gel loading buffer containing 1% (w/v) SDS at 50°C in a water bath. After centrifugation (10 min, 10,000 g at 4°C) the supernatant containing the protein fraction was used immediately, avoiding any freezing-thawing, for SDS-PAGE and western blot detection.

### Reverse Transcription Reaction and PCR

Reverse transcription (RT) was performed with the AMV Reverse Transcriptase (Promega) using total RNA (~1.5  $\mu$ g) and oligo(dT) primer, denatured at 70°C for 10 min, annealing incubation for 5 min at 37°C. The RT reaction was done at 42°C for 90 min, and 72°C 10 min for inactivation. RT-PCR was conducted under standard PCR conditions with the DreamTaq DNA Polymerase (Thermo Scientific) using *ACTIN2* primers (Table S1) to confirm cDNA quality (28 cycles). For the detection of low-abundant transcripts originating from grafted plant tissue (root or shoot) the cDNA samples were submitted to 45 PCR cycles or, as indicated in the legend text, to 50 PCR cycles to ensure lack of presence.

### Quantitative RT-PCR Assays

To measure the levels of mobile and mobile/methylated transcripts, total RNA was submitted to quantitative real-time PCR using an ABI System Sequence Detector (Applied Biosystems 7900HT) as described previously [16]. Three technical replicates were measured for each sample. Thermal cycling was as follows: Step 1: 1 cycle, 2 min at 50°C; Step 2: 1 cycle, 10 min at 95°C; Step 3: 40 cycles, 15 s at 95°C, 1 min at 60°C. Dissociation step: 15 s at 95°C, 15 s at 60°C, 15 s at 95°C. qRT-PCR primers are listed in Table S1.

### Western Blotting

To detect the protein expression levels of YFP-*TCTP1*, YFP-*TCTP1Δ3'*, YFP-*TCTP1Δ5'*, YFP-*TCTP1Δ5'Δ3'*, and YFP-*TCTP1ΔA*, total proteins mixed with loading buffer were boiled at 95°C for 5 min in 1% SDS solution. The samples were separated on 10% SDS-PAGE gel and then transferred to nitrocellulose membranes. The membranes were blocked using 5% low-fat milk in 1xTBS-Tween solution and incubated with 1:10,000 diluted primary antibody 3H9  $\alpha$ -GFP (lot: 50530, ChromoTek) and 1:20,000 diluted anti-rat IgG secondary antibody (Promega). For the detection, the ECL Prime Western Blotting Detection Reagent (GE Healthcare) was used and the chemiluminescent signals were visualized using the ChemiDoc MP Imaging system (Bio-Rad).



### 5-Azacytidine (Aza) Treatment

Transgenic 35S::YFP-TCTP1 and 35S::YFP plants were hypocotyl-grafted with Col-0 roots. Seven days after grafting the plants were transferred to 50 mL Falcon tubes supplemented with 1x MS medium containing 0  $\mu$ M (control), 100  $\mu$ M or 150  $\mu$ M Azacytidine (Stock 50 mM, Sigma) and exposed to long day conditions (16h light / 8h dark; 21°C) on a shaker (90 rpm) for 14 days. CLSM images were taken as described below.

### Microscopy

To detect the presence of YFP-TCTP1 fusions in transgenic and grafted *Arabidopsis* plants 10 days after grafting for YFP fluorescence distribution we used either a Leica SP5 or a Leica SP8 confocal laser scanning microscope (CLSM) as described [16]. In general, the CLSM settings for the detection of YFP fusion constructs and mCherrySKL fluorescence were as follows: Sequential excitation/emission setting; excitation: 30% Argon laser 514 nm / 565 nm; emission detection: detection channel 1 (YFP / Green), 524 to 550 nm; detection channel 2 (mCherry, Propidium iodide / Red), 584 - 615 nm; detection channel 3 (auto-fluorescence, plastids / Blue), 700 - 800 nm; gain (PMT), 500v-750v; pinhole 1.0 (or lower). For high-sensitive detection of YFP a HyD detector was selected as detection channel 1 (> 100% gain) with the according YFP excitation/detection wavelength settings to assess presence of low abundant YFP fluorescent signals in grafted plants. XYZ and YXZ stack images were assembled and processed using the Fiji software package [51].

### Analysis of mRNA Stability

Two-weeks-old wild-type and *dnmt2 nsun2b* mutant seedlings grown on 1/2 MS plates (short day, 8 h/16 h) were harvested and incubated in liquid MS medium containing 10 mM actinomycin D (Sigma) or DMSO (mock treatment) for different time periods. Total RNA was extracted and submitted to reverse transcription and quantification of gene expression levels as described [31].

## QUANTIFICATION AND STATISTICAL ANALYSIS

### Data Processing and Statistical Analysis

Statistical significance of the overlap of two sets of genes and the enrichment of mobile genes or motifs was calculated using exact hypergeometric probability or the hypergeometric test, respectively. The overlap of three set of genes was calculated using the R package SuperExactTest [57]. These overlaps refer to Figures 1A, 1C, 1D, and S1 and are shown in the figures, figure legends and the results section where the figures are described. TLS predictions mentioned in the results section were performed using RNAMotif with the provided tRNA structure descriptor and default parameter settings as previously described [16]. Motif identification as presented in Figure S1C and Results was performed with DREME [33] and the statistical significance was calculated automatically by the algorithm. Standard Errors (SE) and standard deviations (SD) were calculated using Microsoft Excel standard software.

### Quantitative RT-PCR

The statistical analysis of the qRT-PCR assays shown in Figures 3C, 3D, and S3E was performed using two-tailed student's T-Test for two samples with equal variance and three technical replicates.

### Plant Growth Quantification

The statistical details such as number of plants biological replicates, standard error means and significant analysis can be found in the respective figures and figure legends. In Figures 5B and 5C graphs were created using SigmaPlot (version 14.0.) with vertical Box-Plot Graph default calculation settings. The statistical significance of the root number and length differences between the various graft combinations were calculated using two-tailed student's T-Test for two samples with unequal variance. The number of analyzed plants (n) is shown in Figure 5B. Rosette growth measurements and statistics shown in Figure S5C were done as described [58].

## DATA AND CODE AVAILABILITY

No new codes were generated in the study. The datasets generated and analyzed during the current study are available in the NCBI Sequencing Read Archive (SRA) under BioProject ID PRJNA498623.